A Thesis

0n

ENGINEERED NANOSTRUCTURES FOR ACTIVE TARGETING OF CANCEROUS TUMORS

Submitted in the partial fulfilment of requirement for the award of the Degree of

Master of Technology

In

MATERIALS AND METALLURGICAL ENGINEERING

Submitted by

KHUSHWINDER SINGH

Roll No- 600902016

Under the supervision of

Dr. B.N. Chudasama

(Assistant professor)

SCHOOL OF PHYSICS AND MATERIAL SCIENCES

THAPAR UNIVERSITY

PATIALA-147001

JULY-2011

CERTIFICATE

I hereby certify that the work which is being presented in the thesis entitled, ***"Engineered Nanostructures for Active Targeting of Cancerous Tumors"*** *submitted by* ***Mr. KHUSHWINDER SINGH****, Roll No. 600902016 in the partial fulfillment of the requirements for the award of degree of* ***MASTERS OF TECHNOLOGY*** *in* ***"Materials and Metallurgical Engineering"*** *from the* ***School of Physics and Material Science*** *of* ***Thapar University, Patiala****, is an authentic record of his own work carried out under the supervision of Dr. B.N. Chaudasama and refers other researcher's works which are duty listed in the reference section.*

(Dr. B.N. Chudasama)
Supervisor
School of Physics and Material Science
Thapar University
Patiala-147001
India

Countersigned by:

Dr. O. P. Pandey
Professor and Head
SPMS
Thapar University
Patiala, Punjab
India

Dr. S. K. Mohapatra
Dean of Academic Affairs
Thapar University
Patiala, Punjab
India

ACKNOWLEDGEMENT

At this momentous occasion of binding my thesis, I would like to acknowledge the contribution of all those benevolent people, I have been blessed to associate with. Behind every student, there stand a myriad of people whose help and contribution makes things successful. Since such a list can be prohibitively long, I may be excused for any omissions. My first and foremost offering of thanks goes to the architect who shaped my dreams into reality, my guide **Dr. B.N. Chudasama, Assistant Professor, School of Physics and Material Science**. Perseverance, exuberance, positive approaches are just some of the traits they imprinted on my personality. He steered me through their journey through their invaluable advice, positive criticism, stimulating discussion and consistent encouragement. His meticulous attention towards my proceedings, devoted time and his ideas has enabled me to make the project a success. His faith in me always made me more confident. It had been my privilege to work under his guidance.

My greatest thanks are to **Dr. O.P. Pandey, Professor and Head, School of Physics andMaterial Science** for his encouragement and execution of thesis work. I would also like to thank **Dr. Kulvir Singh, Associate Professor, School of Physics and Material Science**, who have been a constant source of inspiration for me throughout this project work. My special thanks to Lab Supdt. (SPMS), **Mr. Purshottam**. His assistance and partnership were of great pleasure.

I would like to convey my sincere gratitude to my friends **Ms. Chandani Khurana, Mr. Paramjyot Jha, Mr. Praveen Jha, Mr. Ishvdeep Singh, Ms. Samita Thakur, Mr. Harjinder Singh, Ms. Kamaldeep Kaur, Ms. Shevali Gargand Mrs. Gurbinder Kaur Chaudhary** for their support, timely help and valuable discussions.

I owe my sincere thanks to all the staff members of School of Physics and Material Science for their support and encouragement. The meaning of my life and work is incomplete without paying regards to my family whose blessings and continuous encouragement have shown me the path to achieve my goals. And above all, I pay my regards to the Almighty for his love and blessings.

Khushwinder Singh

(Khushwinder Singh)

ABSTRACT

The unusual magnetic properties exhibited by superparamagnetic nanoparticles and their promising technological applications have attracted much interest in recent years. The superparamagnetic nanoparticles have applications in the field of nanomedicine ranging from cell separation, hyperthermia to drug delivery. The present thesis is aimed at design and fabrication of magnetic drug delivery system, which is based on active targeting concept. The core of the drug delivery system was comprised of superparamagnetic magnetite nanoparticles. The magnetite nanoparticles were prepared by chemical co-precipitation and thermal decomposition methods. Magnetite nanoparticles have a large surface area/volume ratio and tend to agglomerate to reduce surface energy. To prevent the particle agglomeration we coat magnetite nanoparticles with biocompatible hydrophilic polymer PEG. It was found that the co-precipitation route yield polydisperse system with inferior magnetic properties, while the thermal decomposition route yields monodisperse magnetite with very high saturation magnetization (Ms = 80 emu/g). To provide specificity to the drug delivery system, PEG functionalized magnetite nanoparticles were further modified with folate receptors. This will particularly improve the targeting ability of the system, as the folate receptors are over expressed by most of the cancer tumors and marginally expressed on the surface of healthy cells. The anticancer drug doxorubicin was loaded into the folic acid modified, PEG coated magnetite nanostructures, as doxorubicin is powerful anti-neoplastic drug used for the treatment of wide variety of cancers. The designed drug delivery system and their components were characterized by X-ray diffraction (XRD), Transmission electron microscopy (TEM), Fourier transform infrared spectroscopy (FTIR), UV-visible spectroscopy and Vibrating sample magnetometer (VSM). X-ray analysis reveals that the single phase inverse spinel magnetite nanoparticles have been synthesized both by chemical coprecipitation and thermal decomposition routes. However, TEM and VSM measurements indicate that the co-precipitation method yields polydispersed nanoparticles with poor magnetic properties. The loading of doxorubicin was confirmed by UV-spectra while the surface functionalization of magnetite was confirmed by FTIR spectroscopy. The designed drug delivery system can be

intravenously injected and could be targeted to the desired site by means of external magnetic field. Further, it is also possible to load multiple anticancer/radiotherapeutic drugs into the same drug delivery system.

CONTENTS

LIST OF FIGURES

LIST OF TABLES

CHAPTER-1
INTRODUCTION

Cancer remains one of the leading causes of death in most parts of the world [1]. Early prognosis of the disease due to regular screening and better understanding of the pathophysiology of tumor progression has opened many new vistas as therapy options. In most solid tumors, after its surgical removal, the remaining cancer cells are managed with a variety of treatment options including, radiotherapy, chemotherapy, immunotherapy, etc [2]. However, once the cancer is metastasized, the treatment options are limited, and chemotherapy remains the choice of treatment. The main reason for failure of chemotherapy is the poor accessibility of anti-neoplastic agents to the tumor, requiring higher doses, and then on selective nature of these agents causes severe toxicity [3]. Thus, targeted drug delivery holds immense potential to improve the treatment of cancer by selectively providing therapeutically effective drug concentrations at the tumor site.

1.1 Need for Targeted Drug Delivery

Over the past few decades, our knowledge on the aetiology of cancer has increased exponentially [4]. This improved understanding of the processes that are at the heart of malignant transformation and tumorigenesis has resulted in the development of several new classes of antitumor therapeutics. In addition to classical chemotherapeutic agents (like doxorubicin, cisplatin and paclitaxel), these so-called ‘molecularly targeted therapeutics’ (like growth factor receptor inhibitors, proteasome inhibitors, histone deacetylase inhibitors and antiangiogenic agents) have enriched the therapeutic armoury with their ability to more selectively interfere with certain ‘hallmarks of cancer’. An important, but often neglected property that such second-generation agents share with classical chemotherapeutic drugs, however, is their unfavourable biodistribution upon intravenous administration: the agents are generally rapidly cleared from the circulation, and only a very small fraction reaches the tumor site. Moreover, in certain situations, reaching the tumor is not enough: the drug may be cleared from the tumor too rapidly and may not be available long enough to display a strong therapeutic effect. Also, the physicochemical properties of the drug may make it difficult for the drug to enter the target cells. Tumor-targeted

nanomedicines are drug delivery systems being developed in oncology to improve drug performance by overcoming such limitations [5]. Their most striking feature is their ability to target a drug to the tumour site, thereby enhancing tumoral drug levels, and/or to direct a drug away from those body sites that are particularly sensitive to the toxic effects of the drug.

1.2 Drug Targeting

Drug therapy for the treatment of tumors is often limited by a narrow therapeutic index. One approach that overcomes this limitation is the active targeting of tumors with particulate drug carriers. The derivatization of particulate drug carriers with a ligand leads to the selective targeting of the particulate to selected cells, thereby focusing drug delivery. In addition, particulate drug carriers have a high loading capacity, do not need covalent conjugation of the drug and the formulation protects the entrapped drug from enzymatic inactivation. Despite these favourable properties, their therapeutic efficacy in animal models has been reported only in recent years. The use of internalizing ligands and the targeting of intravascular tumor cells and endothelial cells of tumor blood vessels have been instrumental in demonstrating the clinical effectiveness of particulate drug carriers in animal models. As a result, several actively targeted particulate carriers have now entered into clinical investigation [6].

The rapid increase in understanding of molecular pathogenesis of diseases and emergence of newer techniques in the field of molecular biology has produced an over-abundance of molecular information. Indeed, the pace of these developments has been such that a lot of molecular targets for drug action have been identified at a rate far exceeding our present abilities to utilize this molecular information. Currently, numerous efforts are in progress to discover and develop drugs, which specifically interfere with various signal transduction pathways present exclusively in cancer cells and thus, offer opportunities to tailor individualized treatments based on the unique set of molecular targets produced by the patient's tumor.

Drugs can be delivered either by themselves or in a drug delivery system targeted to specific organs where tumor is residing or specifically to the cancer cell surface [7]. The major components of such a targeted drug delivery include: the

presence of specific targets, ligands for these targets, and ways of delivering the drug to its target using different delivery systems conjugated to the ligands. Solid tumors present a heterogeneous and dynamic biology, which keeps changing with time and thus offers further challenges for drug delivery [8]. A thorough understanding of the tumor cell biology, microenvironment of tumor cells, and their growth patterns allow developing effectively targeted drug delivery options. Drug targeting can be achieved by taking advantage of the distinctive pathophysiological features of a tumor tissue or by actively targeting drug carrier by making use of some target specific ligands.

The concept of targeted drugs is not new, but dates back to 1906 when Ehrlich [9] first postulated the 'magic bullet'. The durability of this concept is a strong indication of its appeal, but the 'magic bullet' continues to be a challenge to implement in the clinic. The challenge has been on three fronts: finding the proper target for a particular disease state; finding a drug that effectively treats this disease; and finding a means of carrying the drug in a stable form to specific sites while avoiding the immunogenic and nonspecific interactions that efficiently clear foreign material from the body. Nanoparticles are potentially useful as carriers of active drugs and, when coupled with targeting ligands, may fulfill many attributes of a 'magic bullet'.

Nanoparticulates encompass a variety of submicron (< 1 μm) colloidal nanosystems, which may be inorganic, liposomal, or polymer [10] i.e. Nanoparticulate drug delivery systems have been studied for several decades now, and many of the features that make them attractive drug carriers are well known. One of the major advantages of nanoparticles is their small size, which allows them to pass through biological barriers. A second advantage is that a high density of therapeutic agent can often be encapsulated, dispersed, or dissolved within these nanoparticles, which depending on the preparation process can be engineered to yield different properties and release characteristics for the entrapped agent. Because of the versatility of chemistries and preparation methods in these systems, surface functionalities can sometimes be incorporated into the nanoparticle. This facilitates additional attractive properties, such as the attachment of 'shielding' ligands that prolong the circulation of the nanoparticles in the blood stream, or the targeting of ligands for interaction with specific cells or tissue.

1.3 Targeting Modalities

There are three types of targeting modalities:

1) Passive targeting
2) Active targeting
3) Magnetic drug targeting

1.3.1 Passive targeting

Tumor-targeted nanomedicines are currently in clinical use. Most of these systems utilise the so-called 'passive targeting'. Passive targeting refers to the substantial extravasation of the nanomedicine-associated drug into the interstitial fluid at the tumour site, exploiting the locally increased vascular permeability. In addition, solid tumours tend to lack functional lymphatic's, and extravasated materials are retained within the tumour site for prolonged periods of time. The exploitation of this so-called 'enhanced permeability and retention' (EPR) effect is currently the most important strategy for improving the delivery of low-molecular-weight chemotherapeutic agents to tumors [11].

Passive targeting approaches make use of the anatomical and functional differences between the normal and the tumor vasculature to allow a selective accumulation of drugs at the tumor site [12]. Passive delivery may be targeted to tumors. Aggressive tumors inherently develop leaky vasculature with 100-800 nm pores due to rapid formation of vessels that must serve the fast-growing tumor. This defect in vasculature coupled with poor lymphatic drainage serves to enhance the permeation and retention of nanoparticles within the tumor region. This is often called the EPR effect [13, 14]. This phenomenon is the basis for 'passive targeting'.

EPR Effect

Tumor vasculature is generally, more heterogeneous in distribution, larger in size, and more permeable than the vasculature present in normal tissues [15, 16]. Unlike the tight endothelium of normal blood vessels, the vascular endotheliums in tumor microvessels are discontinuous and leaky. It has been determined that the size of gaps

between the endothelial cells ranges from 100-780 nm depending on the anatomic location of tumor [17, 18]. Further, the elevated levels of growth factors like VEGF (vascular endothelial growth factor), bFGF (basic fibroblast growth factor) in tumor vasculature result in vasodilation and enhance the extravasation of drugs in tumors [19]. This coupled with the impaired lymphatic drainage in solid tumors allows an enhanced accumulation and retention of high molecular weight drugs in solid tumors, popularly known as the enhanced permeability and retention (EPR) effect [20, 21]. Factors which influence EPR include the size of tumors, degree of tumor vascularisation, and angiogenesis [22]. Thus the stage of the disease is critical for drug targeting using EPR effect.

Two liposomal formulations, which target drugs to tumors by means of EPR effect, are currently available commercially. Daunosome™ liposome (NeXtar, Inc.) encapsulating daunorubicin and Doxil™ (Sequus Pharmaceuticals) based on doxorubicin, are sterically stabilized liposomal formulations with extended circulation times which efficiently accumulate in the tumor cells. This passive targeting of anthracycline anti-cancer agents results in reduced drug levels in plasma and thus, minimizes the frequently occurring cardiac adverse effects of these drugs [23].

The interstitial fluid pressure is high in the center of tumor and relatively low in the periphery and the surrounding tissues. Thus, there is a substantial permeation of macromolecules in the peripheral regions of a tumor mass, in contrast to relatively less drug diffusion into the center of solid tumors. For these macromolecules to diffuse into the more necrotic interior regions of the tumor, they have to overcome the outward flow of interstitial fluid, which can carry these drugs by convection to normal tissues [2]. Thus, the systems, which make use of the EPR effect need to be optimized for deep tumor penetration or some adjunctive physiological modulators, can be co-administered to increase the tumor blood flow. VEGF, bFGF, angiotensin converting enzyme inhibitors like enalapril can variably increase the tumor blood flow and thus the tumor penetration of drugs [20, 24]. However, there are limitations to the use of the above mentioned growth factors due to their involvement in tumor growth and metastasis. Further, these theoretical options have not yet been confirmed in clinical settings.

1.3.2 Active targeting

In active drug targeting, ligands are attached to drug delivery systems to act as homing devices for binding to receptor structures expressed at the target site [25, 26]. Antibody drug conjugates targeted to, T-cell lymphoma and acute myeloid leukaemia, respectively, have been successfully used for delivering radionuclides, immunotoxins and antitumor antibiotics more selectively to tumour cells. Antibodies, antibody fragments and peptides have also been used as targeting moieties for drug delivery systems. Active targeting of particulates that carry physically entrapped drugs can achieve drug delivery to target cells *in vivo*, thus maximizing the therapeutic efficacy of the drug and reducing its systemic side-effects. To attain active targeting of a drug carrier, particulates are derivatized with ligands that bind to specific receptors expressed on target cells. On binding to the receptors, the ligand–particle complex could be internalized into the cell or remain cell-bound without being internalized [6].

An important class of targets is receptors involved in the uptake of vitamin B12, folic acid, biotin, and thiamine [27]. These are differentially overexpressed on the surface of cancer cells, which creates a possible target for several types of cancer, including ovarian, breast, lung, renal, and colorectal cancers [28].

Folate Receptor Targeting

Folic acid is a vitamin that is essential for the biosynthesis of nucleotides. It is consumed in elevated quantities by proliferating cells and is transported across the plasma membrane using either the membrane-associated reduced folate carrier or the folate receptor (FR). The former is found in virtually all cells; the latter is found primarily on polarized epithelial cells and activated macrophages [29]. The reduced folate carrier is probably capable of internalizing the necessary folate in normal cells, however, FR is frequently overexpressed on tumor cells as a consequence of increased folate requirements, and furthermore increases with advancing stages of the disease [30]. *In-vitro* experiments using folate-coated liposomes with encapsulated doxorubicin have shown that KB and HeLa cells, which vastly over-express the FR, show significant uptake of the drug [31]. Saul et al. [32] have synthesized a DPPE-PEG2000-folate conjugate and inserted this lipid into pre-formed doxorubicin loaded

liposomes by simple mixing. They found that KB cells, which express high amounts of the FR, have a maximum uptake of doxorubicin at 700 folate ligands per liposome. Leamon et al. [33] have recently evaluated the in vitro and in vivo status on the delivery of oligonucleotides encapsulated in folate-coated liposomes. Delivery of the oligonucleotides in vitro was very efficient, whereas in vivo delivery results were less promising. However, FR targeted liposomes have proven effective in delivering doxorubicin in vivo [34, 35] and have been found to bypass multidrug resistance in cultured tumor cells [36].

1.3.3 Magnetic Drug Targeting

Magnetically targeted drug delivery by particulate carriers is an efficient method of delivering drugs to localized disease sites, such as tumors. High concentrations of chemotherapeutic or radiological agents can be achieved near the target site without any toxic effects to normal surrounding tissue. Non-targeted applications of magnetic microspheres and nanospheres include their use as contrast agents (MRI).

1.3.3.1 Principle

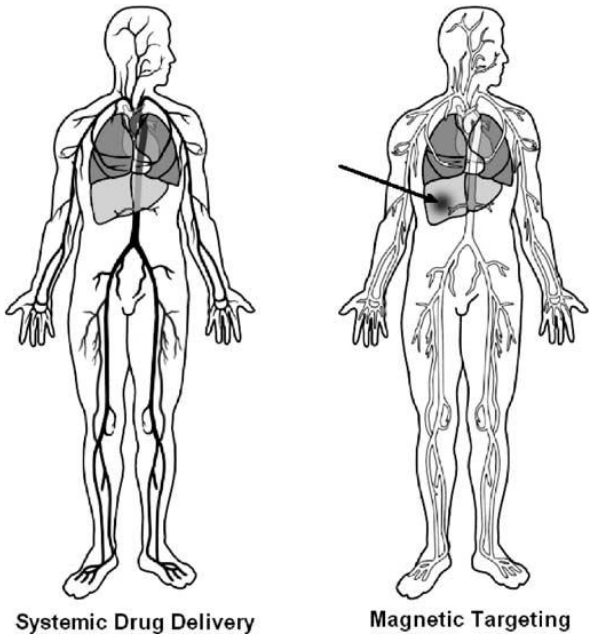

Figure 1.1 Concept of magnetic drug targeting

Figure 1.1 highlights the concept of magnetic targeting. In magnetic targeting, a drug or therapeutic radioisotope is bound to a magnetic compound, injected into a patient's blood stream, and then stopped with a powerful magnetic field in the target area (Figure 1.1). Depending on the type of drug, it is then slowly released from the magnetic carriers or confers a local effect. It is thus possible to replace large amounts of freely circulating drug with much lower amounts of drug targeted magnetically to localized disease sites [37].

Magnetic carriers receive their magnetic responsiveness to a magnetic field from incorporated materials such as magnetite, iron, nickel, cobalt, neodymium–iron–boron or samarium–cobalt (see Figure 1.2). Magnetic carriers are normally grouped according to size. At the lower end, we have the ferrofluids, which are colloidal iron oxide solutions. Encapsulated magnetite particles in the range of 10–500 nm are usually called magnetic nanospheres and any magnetic particles of just below 1–100 nm are magnetic microspheres.

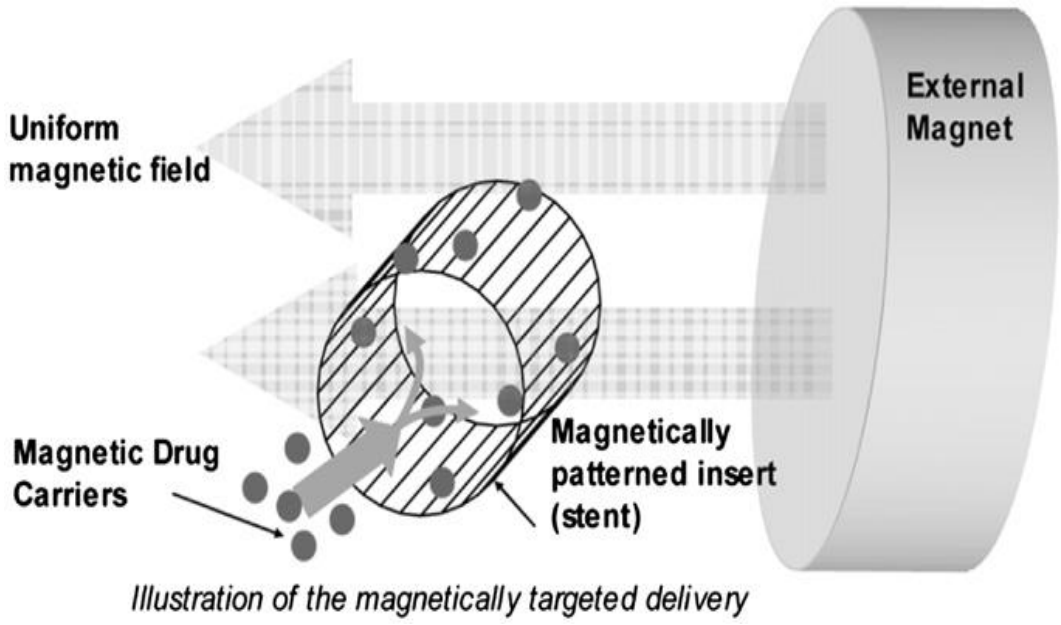

Figure 1.2 A schematic representation of the implant-based magnetic drug delivery system

For biomedical applications, magnetic carriers must be water-based, biocompatible, nontoxic, and nonimmunogenic. Improved biocompatibility however,

was reached by encapsulating the magnetic materials. The “shell” material determines the reaction of the body to the microsphere. Matrix materials that have been tested for the magnetic microsphere include chitosan, dextran, poly(lactic acid), starch, poly(vinyl alcohol), polyalkylcyanoacrylate, polyethyleneimine, polysaccharides, gelatine and proteins.

1.3.3.2 Applications of magnetic drug targeting

1) <u>Magnetic delivery of chemotherapeutic drugs to liver tumors</u>

The first clinical cancer therapy trial using magnetic microspheres (MMS) was performed by Lübbe et.al. [38] in Germany for the treatment of advanced solid cancer in 14 patients. Their MMS were small, about 100 nm in diameter, and filled with 4-epidoxorubicin. The phase I study clearly showed the low toxicity of the method and the accumulation of the MMS in the target area. However, MRI measurements indicated that more than 50 % of the MMS had ended up in the liver. This was likely due to the particles’ small size and low magnetic susceptibility which limited the ability to hold them at the target organ.

The start up company FeRx in San Diego developed irregularly shaped carbon-coated iron particles of 0.5–5 μm in diameter with very high magnetic susceptibility and used them in a clinical phase I trial for the treatment of inoperable liver cancer [39]. They have treated 32 patients to date and are able to super-selectively (i.e. well directed) infuse upto 60 mg of doxorubicin in 600 mg MMS with no treatment-related toxicity [40]. The firm recently started a large phase I/II trial for the treatment of hepatocellular carcinoma in China, Korea, and the US [40].

2) <u>Treatment of tumors with magnetically induced hyperthermia</u>

Magnetic Hyperthermia is a promising approach for cancer treatment that uses AC magnetic field to heat target areas (cancer tissue). Magnetic hyperthermia provides the heat at the site of the tumor invasively by applying an external alternating magnetic field to the magnetic particles at the tumor site. The particles will heat up and conduct

the heat to the tumor cells. The use of materials with Curie temperature in the range of 41– 46 $^{\circ}$C is desired to provide a safeguard against over heating of normal cells, due to the decrease of magnetic coupling in the paramagnetic regime (above T_c).

The method relies on the theory that any metallic objects when placed in an alternating magnetic field will have induced currents flowing within them. The amount of current is proportional to the size of the magnetic field and the size of the object. As these currents flow within the metal, the metal resists the flow of current and thereby heats, a process termed inductive heating. If the metal is magnetic, such as iron, the phenomenon is greatly enhanced. Therefore, when a magnetic fluid is exposed to an alternating magnetic field the particles become powerful heat sources, destroying the tumor cells [41].

Developments by Jordan and Chan led to the current hyperthermia application of single domain, dextran-coated magnetite nanoparticles in tumors [42, 43]. The first clinical trial is ongoing in Germany [44]. Magnetic hyperthermia is also possible with larger magnetic particles, as shown by the group of Moroz [45]. Their 32 μm plastic particles contain maghemite and embolize the arterial blood supply of the tumor, in addition to the magnetic hyperthermia treatment. In an animal study with 10 rabbits, the tumor volumes decreased by 50–94 % within 2 weeks. Ongoing investigations in magnetic hyperthermia are focused on the development of magnetic particles that are able to self-regulate the temperature they reach. The ideal temperature for hyperthermia is 43–45 $^{\circ}$C, and particles with a curie temperature in this range have been described by Kuznetsov [46].

3) <u>Magnetic control of pharmacokinetic parameters and drug release</u>

The magnetic component in microspheres can also be used for purposes other than targeting. Langer embedded magnetite or iron beads into a drug-filled polymer matrix and then showed that they could activate or increase the release of the drug from the polymer by moving a magnet over it or by applying an oscillating magnetic field [47]. The micro-movement within the polymer seemed to have shaken the matrix or produced “micro-cracks” and thus made the influx of liquid, dissolution and efflux of the drug possible.

In this way, it was possible to magnetically activate the release of insulin from a depot underneath the skin [48]. Done repeatedly, this would allow for pulsatile drug delivery. Another mechanistic approach based on magnetic attraction is the slowing-down of oral drugs in the gastrointestinal system. This is possible by filling an additional magnetic component into capsules or tablets. The speed of travel through the stomach and intestines can then be slowed down at specific positions by an external magnet, thus changing the timing and/or extent of drug absorption in stomach or intestines. Slowing down the passage of magnetic liposomes with a magnet actually increased the blood levels of a drug [49].

4) <u>Magnetic targeting of radioactivity</u>

Magnetic targeting can also be used to deliver therapeutic radioisotopes [50]. The advantage of this method over external beam therapy is that the dose can be increased, resulting in improved tumor cell eradication, without harm to nearby normal tissue. Different radioisotopes can treat different treatment ranges depending on the radioisotope used. The emitters 90Y for example will irradiate up to a range of 12 mm in tissue. Unlike chemotherapeutic drugs, the radioactivity is not released, but rather the entire radioactive microsphere is delivered to and held at the target site to irradiate the area within the specific treatment range of the isotope. Once they are not radioactive anymore, biodegradation of the microspheres occurs (and is desired). Initial experiments in mice showed that intraperitoneally injected radioactive poly(lactic acid) based MMS could be concentrated near a subcutaneous tumor in the belly area, above which a small magnet irradiation from the emitter 90Y-containing MMS resulted in the complete disappearance of more than half of the tumors. Magnetic targeted carriers (MTC), which are more magnetically responsive iron carbon particles, have been radiolabeled in the last couple of years with isotopes such as 188Re [50], 90Y, 111In and 125I [40] and are currently undergoing animal trials. As an example, a preliminary in vivo investigation of binding stability and localization was performed in normal swine. Eleven millicurie of 90Y-MTC was administered intra-arterially to a swine liver via catheterization of the hepatic artery. Blood samples were taken following the administration, which indicated that less than 3% of the total injected activity was circulating 30 min following the administration and decreased over time.

5) Other magnetic targeting applications

Similar to chemotherapeutic drugs, many other drugs including peptides and proteins can be adsorbed or encapsulated into magnetic microspheres or nanospheres. Normal pharmaceutical technology is employed to influence release kinetics. Ongoing work describes the encapsulation of the peptide octreotide and the protein tumor necrosis factor alpha (TNF-α) [40].
A very recent development in the field of magnetic targeting is the use of magnetically enhanced gene therapy [51]. Advantages of such an approach are targeted gene transfection at rapid speed and high efficiencies.

It is also possible to use only the mechanical-physical properties of magnetic particles or ferrofluids for therapy. One example is the embolization (clogging) of capillaries under the influence of a magnetic field [52]. In this way, tumors could be specifically starved of their blood supply. Another elegant example is the use of magnetic fluids to prevent retinal detachment, thus preventing the patients from going blind [53]. A magnetized sclera buckle, similar to a rubber band, is placed around the eye. The magnetic fluid is then injected into the eye and immediately drawn towards the buckle by its magnetic forces. The mechanical forces push the retina back into its original place.

CHAPTER-2
LITERATURE REVIEW

Intense research has led to a more comprehensive understanding of cancer at the genetic, molecular, and cellular levels providing an avenue for methods of increasing antitumor efficacy of drugs while reducing systemic side effects. Nanoparticulate technology is of particular use in developing a new generation of more effective cancer therapies capable of overcoming the many biological, biophysical, and biomedical barriers that the body stages against a standard intervention. Nanoparticles show much promise in cancer therapy by selectively gaining access to tumor due to their small size and modifiability. Nanoparticles are prepared to take advantage of fundamental cancer morphology and modes of development such as rapid proliferation of cells, antigen expression, and leaky tumor vasculature. In cancer treatment and detection nanoparticles serve many targeted functions in chemotherapy, radiotherapy, immunotherapy, immunodetection, thermotherapy, imaging, photodynamic therapy, and anti-angiogenesis. Moreover, multifunctional nanoparticles perform many of these tasks simultaneously such as targeted delivery of a potent anticancer drug at the same time as an imaging material to visualize the effectiveness of the drug utilized for treatment follow-up.

Doxorubicin-conjugated biodegradable polymeric micelles having acid-cleavable linkages are discovered by Hyuk Sang Yoo et al. [54]. Doxorubicin was chemically conjugated to the terminal end of a di-block copolymer composed of Poly(L-lactic acid) (PLLA) and methoxy-poly(ethylene glycol) (mPEG) via two acid-cleavable linkages. A hydrazone bond and a *cis*-acotinyl bond were formed between doxorubicin and the terminal group of PLLA segment in the block copolymer. Doxorubicin conjugated PLLA–mPEG di-block copolymers self-assembled to form micelles in aqueous solution. The doxorubicin conjugated micelles were about 89.1 nm in diameter and their critical micelle concentration was 1.3 mg/ml. These values were comparable with those of unconjugated micelles. In an acidic condition, the conjugated doxorubicin in the hydrazone linkage was readily cleaved, releasing doxorubicin in an intact structure. Doxorubicin-conjugated PLLA–mPEG micelles were more potent in cell cytotoxicity than free doxorubicin, suggesting that they were

more easily taken up within cells with concomitant rapid release of cleaved doxorubicin into the cytoplasm from acidic endosomes.

Biodegradable polymeric nanospheres formed by Temperature-induced phase transition in a mixture of Poly(lactide-co-glycolide) and Poly(ethylene oxide)-Poly(propylene oxide)-Poly(ethylene oxide) Triblock copolymer are discovered by Ka Eul Lee et al. [55]. The mixture of poly(ethylene oxide)-poly(propylene oxide)-poly(ethylene oxide) Triblock copolymer **(**F-127) and PLGA (poly(lactide-*co*-glycolide)) forms a liquid state above their phase transition temperatures, and the phase-separated state is induced by decreasing the temperature below the phase transition temperature. On the basis of the temperature-induced phase transition behavior in the mixture of F-127 and PLGA, a novel method for the preparation of drug-loaded PLGA nanospheres was designed and characterized by measuring the loading amount, the encapsulation efficiency, and the drug release pattern.

A Short-term (accelerated release) approach to evaluate peptide release from PLGA depot formulations is developed by Mohammed Shameem et al. [56]. An accelerated method to evaluate peptide release from poly(di-lactide-co-glycolide) (PLGA) depot formulations in short time is described. Peptide-loaded microspheres were made from hydrophilic 50:50 PLGA by a dispersion solvent extraction technique, and peptide release was studied at 37 $^{\circ}$C and at higher temperatures in various media. For all accelerated conditions, release was faster at temperatures above the glass transition, T_g, of the host polymer. Complete release of peptide from 8600 MW PLGA was achieved in 35 h at 50°C in buffered and non buffered media containing 0.5 % polyvinyl alcohol (PVA). Type of release media and concentration of PVA influenced the release profiles. A PVA concentration of 0.1 to 0.5 % was found to prevent aggregation of microspheres at higher temperatures, with an increase in release at the higher PVA concentration. Peptide release was associated with a reduction of pH of the releasing media and increased mass loss. Complete peptide release at pH 4 from 8.6 kd and 28 kd PLGA at 50 and 60 $^{\circ}$C occurred within 30-40 h and correlated well with the real-time release at 37 $^{\circ}$C and pH 7.0. At the higher molecular weight, a slightly longer accelerated release time and higher temperature were required to correlate with the real time release. The data suggest that by optimization of release conditions such as temperature, surfactant concentration,

buffer component and pH, an accelerated study could be employed to evaluate depot formulations for a given polymer type.

SMA–doxorubicin, a new polymeric micellar drug for effective targeting to solid tumors is discovered by Khaled Greisha et al. [57]. Copolymer of styrene-maleic acid (SMA) was used to construct micelles containing doxorubicin by means of a hydrophobic interaction between the styrene moiety of SMA and doxorubicin (Dox). The micelles obtained (SMA–Dox) showed a high solubility in water and a constant doxorubicin release rate of about 3–4 %/day in-vitro. The SMA–Dox micelle preparation was less (36–70 %) cytotoxic to the SW480 human colon cancer cell line in-vitro compared with free doxorubicin. In-vivo assay of SMA–Dox in ddY mice bearing S-180 tumor revealed a potent anticancer effect with no remarkable toxicity up to a dose of 100 mg/kg of free doxorubicin equivalent. The drug concentration in tumor after administration of SMA–Dox was 13 times higher than that after the free drug. This result was attributed to the enhanced permeability and retention (EPR) effect of macromolecular drugs observed in solid tumors. Complete blood counts and cardiac histology showed no serious side effects for intravenous (i.v.) doses of the micellar formulation as high as 100 mg/kg doxorubicin equivalent in mice. These data indicate that i.v. administration of SMA–Dox micellar formulation can enhance the therapeutic effect of doxorubicin while reducing greatly cardiac and bone marrow toxicity, which should allow safe use of high doses of this agent.

How porosity and size affect the drug release mechanisms from PLGA-based microparticles, this study was done by D. Klose et al. [58]. Porous, poly(lactic-*co*-glycolic acid) (PLGA)-based microparticles were prepared using a water-in-oil-in-water (W/O/W) solvent extraction/evaporation technique. Lidocaine was used as a model drug and different-sized particle fractions were obtained by sieving. In contrast to non-porous microparticles of identical composition, the relative drug release rate was found to decrease with increasing system size. SEC, DSC and gravimetric analysis showed that the degradation rate of the polymer increased with increasing microparticle dimension, indicating that autocatalytic effects play an important role even in small and highly porous PLGA-based microparticles. However, these effects were much less pronounced than in non-porous devices. Importantly, they were over compensated by the effects of the increasing diffusion pathway lengths with

increasing system dimension. Thus, high initial microparticle porosities do not only lead to increased drug mobilities, but can also fundamentally alter the underlying mass transport mechanisms.

Thermo responsive core–shell magnetic nanoparticles for combined modalities of cancer therapy are developed by S Purushotham et al. [59]. γ- iron oxide magnetic nanoparticles (MNP) with average sizes of 14, 19 and 43 nm were synthesized by high temperature decomposition. Composite magnetic nanoparticles (CNP) of 43 nm MNP coated with the thermo responsive polymer poly-n-isopropylacrylamide (PNIPAM) were prepared by dispersion polymerization of n-isopropylacrylamide monomer in the presence of the MNP. In vitro drug release of doxorubicin-(dox) loaded dehydrated CNP at temperatures below and above the lower critical solution temperature of PNIPAM (34 $^{\circ}$C) revealed a weak dependence of drug release on swelling behavior. The particles displayed Fickian diffusion release kinetics; the maximum dox release at 42 $^{\circ}$C after 101 h was 41 %. In-vitro simultaneous hyperthermia and drug release of therapeutically relevant quantities of dox was achieved, 14.7 % of loaded dox was released in 47 min at hyperthermia temperatures.

Elevated temperature accelerated release testing of PLGA microspheres are performed by Banu S. et al. [60]. Drug release from four different poly(lactic-co-glycolic) acid (PLGA) microsphere formulations was evaluated under “real-time” (37 $^{\circ}$C) and accelerated release testing conditions of elevated temperature (45, 53, 60 and 70 $^{\circ}$C) and increase in flow rate (4–35 ml/min) using United States Pharmacopeia (USP) apparatus 4. Formulation 5 K (composed of low Mw PLGA) exhibited diffusion-controlled kinetics in “real-time”. Whereas, formulations 25 K, 28 K and 70 K (composed of medium and high Mw PLGA) followed erosion-controlled kinetics at 37 $^{\circ}$C. Temperature induced degradation of the microspheres was studied by monitoring drug release rates, change in molecular weight and morphological changes. Molecular weight change measured by gel permeation chromatography followed first order kinetics for both “real-time” and accelerated release. All four formulations exhibited morphological changes (such as surface pore closing and geometry change) at elevated temperature with consequent reduction in burst release.

Preparation and Characterization of Folic Acid Linked Poly(L-glutamate) nanoparticles for Cancer Targeting was done by Yong-kyu Lee [61]. Nanoparticles of Poly(L-glutamic acid) (PG) conjugated to the anticancer drug paclitaxel and targeted moiety folic acid (FA) were synthesized and characterized in vitro. The nanoparticles were designed to take advantage of FA targeting to folate receptor (FR) positive cancer cells. The amount of paclitaxel conjugated to FA-PG was 25 % by weight. Cellular uptake of the conjugate was FA dependent, and the conjugate uptake was mediated specifically by the folate receptor.

The grafting and release behavior of doxorubicin from $Fe_3O_4@SiO_2$ core–shell structure nanoparticles via an acid cleaving amide bond: the potential for magnetic targeting drug delivery. This study was done by F H Chen and Q Gao [62]. The DOX-loading efficiency determined by UV–vis spectrometer was 86.5 %. Drug release experiments displayed a pH-dependent behavior that DOX was cleaved from the nanoparticles easily under low pH conditions in the presence of protease and that most of the conjugated doxorubicin were released within the first 12 h. The prepared DOX-grafted $Fe_3O_4@SiO_2$ core–shell structure nanoparticles showed a superparamagnetic property with a saturation magnetization value of 49.3 emu g^{-1}, indicating a great potential application in the treatment of cancer using magnetic targeting drug-delivery technology.

3.1 Design of drug delivery system

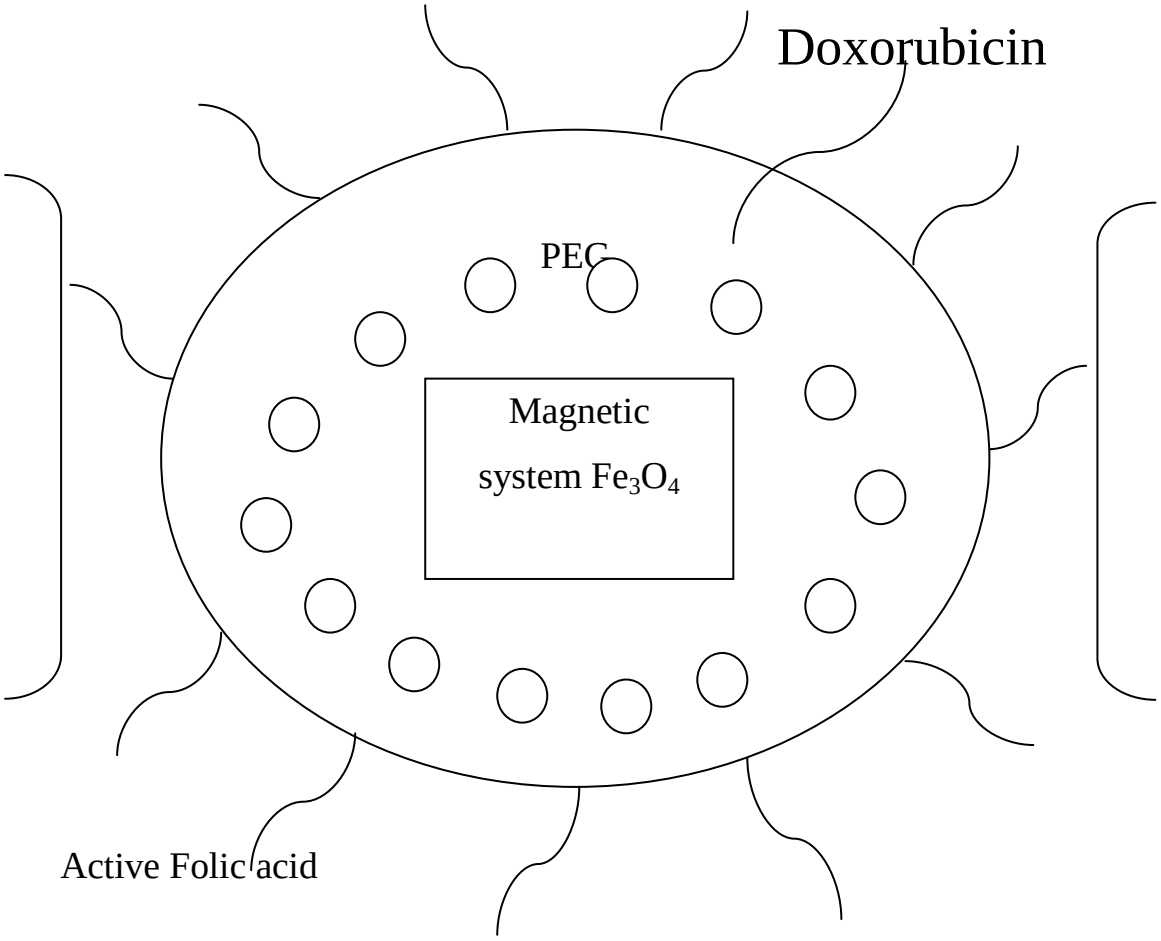

Figure 3.1 Design of drug delivery system

The drug delivery system includes:

1) Magnetic nanoparticles
2) Biocompatible polymeric shell
3) Active targeting ligand
4) Anticancer drug.

3.1.1 Magnetic nanoparticles based systems

The main problems currently associated with systemic drug administration include even biodistribution of pharmaceuticals throughout the body, the lack of drug specificity towards a pathological site, the necessity of a large dose to achieve high local concentration, non-specific toxicity and other adverse side effects due to high drug doses. Drug targeting aims to resolve many of these problems [63]. Amongst the current principle schemes of drug targeting is magnetic targeting, i.e. the targeting of a drug immobilized on magnetic materials under the action of an external magnetic field. To enhance target specificity the drug is associated with another molecule capable of specific recognition and binding to the target site. Target recognition can occur at different levels: on the level of the whole organ, the level of certain specific cell types for a given organ, or on the level of individual components characteristic for these cells such as cell surface antigens. The most common type of associated molecules are antibodies (and their fragments), lectins, proteins, hormones, charged molecules and some low molecular weight ligands such as folate.

We need biocompatible, monodispersed nanoparticles and efficiency of cell targeting by nanoparticles or their conjugates. Monodispersed nanoparticles are necessary because the clusters formed by agglomerated nanoparticles differ magnetically from the individual nanoparticles. Magnetic nanoparticles have a large surface area/volume ratio and tend to agglomerate to reduce surface energy. Agglomerated nanoparticles have a short circulation time in blood, as a result of being quickly eliminated from the blood stream by the macrophages of the mononuclear phagocyte system (MPS) before they can reach target cells or tissues. One of the effective approaches to prevent the particle agglomeration is to coat nanoparticles with biocompatible polymers and the specific targeting is usually achieved by coating the particles with targeting agents [64]. In the present study, the protein-resistive, nonantigenic and biocompatible polyethylene glycol (PEG) has been used to coat nanoparticles and reduce nonspecific protein adsorption that may cause the particles to be cleared by the macrophages. The current approaches for targeting tumor cells typically involve coating nanoparticles with monoclonal antibodies as specific targeting agents to “tumor specific-antigens” on tumor cells. The use of low molecular weight targeting agents such as folic Acid (FA) as surface coatings have

great promise for the specific cancer cell recognition and enhancement in intracellular uptake of nanoparticles. FA is recognised to target specific tumor cells, largely because:

1) Folate receptors are upregulated in many human cancers, including ovary, brain, kidney, breast, myeloid, and lung cancers.
2) Access to the folate receptor in those normal tissues that express it can be severely limited due to its location on the apical (externally facing) membrane of polarised epithelia.
3) Other advantages of FA include its high binding affinity to folate receptors, low immunogenicity, ease of modification, high stability during storage, compatibility with a variety of organic and aqueous solvents, low cost and vast availability.
4) Unlike macromolecular target agents such as widely used antibodies that encounter significant permeability barriers in passing the cell membrane, FA has short chains and a small size, and thus will facilitate the internalization of nanoparticles.

Doxorubicin is a widely used anticancer drug used for the treatment of large variety of cancers. Hence, in the present study, doxorubicin is immobilized on nanoparticle based magnetic drug targeting system.

3.2 Synthesis of magnetic drug delivery system

3.2.1 Materials

Iron acetylacetonate, 1, 2-hexadecanediol, oleylamine, dicyclohexyl carbodiimide and folic acid were purchased from Sigma-Aldrich. Oleic acid, diphenyl ether, nitric acid, ferrous sulphate, PEG 600, dimethyl sulphoxide and ammonia were purchased from S. D. fine Chem. Ltd. Ethanol, n-hexane and HPLC grade water were purchased from MERCK. Ferric chloride was purchased from Loba Chemicals Ltd. Doxorubicin hydrochloride was purchased from Fresenius Kabi Oncology Ltd. Distilled water was obtained locally. All materials were used as received without further purification.

3.2.2 Synthesis of magnetite nanoparticles

Different methods are used to synthesize magnetite nanoparticles like thermal decomposition, sol-gel, microemulsion, reverse micelle, spray pyrolysis, chemical co-precipitation. In the present study magnetite nanoparticles are synthesized by thermal decomposition and chemical co-precipitation routes.

3.2.2.1 Synthesis of magnetite nanoparticles by chemical co-precipitation method

In a typical synthesis, stoichiometric aqueous mixture of ferric (5 mM) and ferrous (2.5 mM) ions were prepared using 0.05M ferric chloride ($FeCl_3.6H_2O$) and 0.01M ferrous sulphate ($FeSO_4.7H_2O$). The color of mixture was brown. In these solutions 20 mM aqueous solution of ammonium hydroxide was added drop-wise under continuous stirring. Black precipitates were formed immediately. The pH of the slurry was maintained at 10.5 by adding excess ammonia. After continuous stirring for 20 min at room temperature (300 K), the black precipitates were magnetically decanted and washed several times with warm distilled water to remove the unreacted residues and water soluble impurities. The following chemical reaction takes place during synthesis:

$$2\ FeCl_3.6H_2O + FeSO_4.7H_2O + 8NH_4OH \rightarrow Fe_3O_4 + 6NH_4Cl + (NH_4)_2SO_4 + 23H_2O$$

This method yields polydispersed nanoparticles.

3.2.2.2 Synthesis of magnetite nanoparticles by thermal decomposition method

Magnetite nanoparticles were prepared by high-temperature decomposition of iron acetylacetonate. This will yield monodispersed magnetite nanoparticles. First, 20 mL diphenyl ether, 0.71 g iron (III) acetylacetonate, 2.58 g 1, 2-hexadecanediol, 1.9 mL oleic acid, and 2 mL oleylamine were thoroughly mixed by magnetic stirring in a 250 mL three-necked flask. The solution was heated to 200 $^{\circ}$C at a rate of 50 $^{\circ}$C/h. It was dwelled at 200 $^{\circ}$C for 2 h. During this time homogenous nucleation of magnetite took place. After 2 h, the temperature of the solution was rapidly raised to 260 $^{\circ}$C. It was refluxed at this temperature for another hour. During this process, the initial brown-

black color of the solution changed to dark black, implying the growth of the magnetite nanoparticles. Subsequently, the resultant solution was cooled to room temperature, and 40 mL ethanol was added to obtain a black precipitate. The black magnetite precipitates were separated by centrifuging at 10,000 rpm for 30 min. Purification of magnetite nanoparticles and preventing their agglomeration was accomplished using the following outlined experimental steps.

The black precipitates were redispersed in 20 mL hexane to obtain a non-transparent homogeneous solution. The homogeneous solution was centrifuged at 6000 rpm for 10 min and residues (if any) were removed. The solution containing magnetic nanoparticles was again precipitated with 20 mL ethanol, centrifuged at 10,000 rpm for 10 min and the purified magnetite nanoparticles were dried @ 300 K for 24 h. The surface property of the magnetic nanoparticles is important because the surface is subsequently modified with biocompatible hydrophilic polymer for use as a drug carrier. Thus, the magnetic nanoparticles were dialyzed for 2 days against 0.01 M nitric acid and stored at 4 $^{\circ}$C for subsequent functionalization with hydrophilic polymer.

3.2.3 Functionalization of magnetite nanoparticles with PEG

3.2.3.1 PEG-functionalization of polydispersed magnetite nanoparticles

In order to obtain optimum concentration of PEG, polydispersed magnetite nanoparticles were coated with different amounts of PEG. The w/w ratio of PEG:Fe_3O_4 was kept as 1:1, 1:2 and 1:4. In a typical experiment, requisite amount of PEG 600 was dissolved in 100 mL distilled water. To this polydispersed magnetite nanoparticles were added. The solution was stirred for 8 h. During this time, a fine layer of PEG was coated on the surface of magnetite nanoparticles. PEG coated magnetite nanoparticles were recovered from the solution by magnetic decantation, washed five times with distilled water and dried at room temperature.

3.2.3.2 PEG-functionalization of monodispersed magnetite nanoparticles

To functionalize PEG on monodispersed magnetite nanoparticles the dialyzed magnetite nanoparticles were mixed with PEG solution in PEG:Fe_3O_4 w/w ratio of

1:2. A low ratio was preferred to avoid encapsulation of nanoparticles with a thicker layer of PEG. In a typical experiment, 140 mg of PEG 600 was dissolved in 80 ml of HPLC water and pre-synthesized monodisperse magnetite nanoparticles were added to it. The solution was stirred for 8 h. The resulting solid product was washed five times with distilled water and dried at room temperature.

3.2.4 Folic acid modified PEG-coated magnetic nanoparticles

Specific targeting is achieved by coating the nanoparticles with targeting agents. The use of low molecular weight targeting agents such as folic Acid (FA) as surface coatings have great promise for the specific cancer cell recognition and enhancement in intracellular uptake of nanoparticles [61].

We attach folic acid to monodisperse PEG coated magnetite nanoparticles because the polydisperse magnetite nanoparticles have poor response in targeting experiment because of the inferior magnetic properties. The attachment of folic acid on PEG coated magnetite nanoparticles are mainly based on the reaction between amino and carboxyl groups to form amide bonds. Folic acid is generally difficult to conjugate to the surface of the polymer because of the weak chemical reactivity of the carboxylic acid group associated with the PEG. Hence, carboxyl group of folic acid was first activated with dicyclohexyl carbodiimide (DCC) [65]. First, 9 mg of folic acid was dissolved in 10 mL dimethyl sulphoxide (DMSO). Second, DCC was added to the solution corresponding to a folic acid:DCC w/w ratio of 1:1 and sonicated for 2 h. In the last stage, PEG-coated magnetite nanoparticles was added and again sonicated for 2 h. The folic acid-modified, PEG coated magnetite nanoparticles were then washed thrice with distilled water and dried. This entire reaction was carried out in dark.

3.2.5 Conjugation of drug to functionalize magnetite nanoparticles

The anticancer drug doxorubicin (1 mL) was dissolved in 10 mL of distilled water. Folic acid-modified, PEG encapsulated magnetite nanoparticles were mixed with 10 mL drug solution. The resulting solution was placed on a rotary shaker (200 rpm) for 2 h at room temperature. This reaction was also carried out in dark. The drug-conjugated, folic acid-modified, PEG-coated magnetic nanoparticles were then

washed with distilled water until no residue of doxorubicin was detected in UV spectra.

A schematic of the different steps in the synthesis of drug-conjugated, folic acid-modified, PEG-coated magnetite nanoparticles are summarized as follows:

Step 1: Functionalization of Fe_3O_4 with PEG polymer

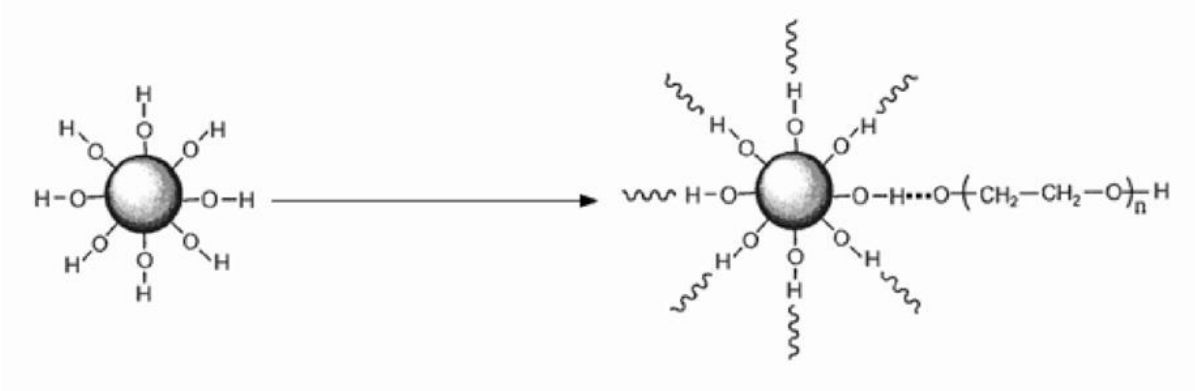

Fe_3O_4 PEG-functionalized Fe_3O_4

Step 2: Activation of Folic acid using DCC

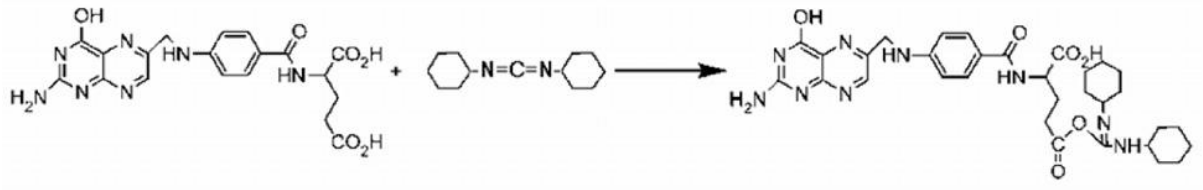

Folic acid DCC Activated folate

Step 3: Attaching activated folate to PEG-functionalized Fe_3O_4

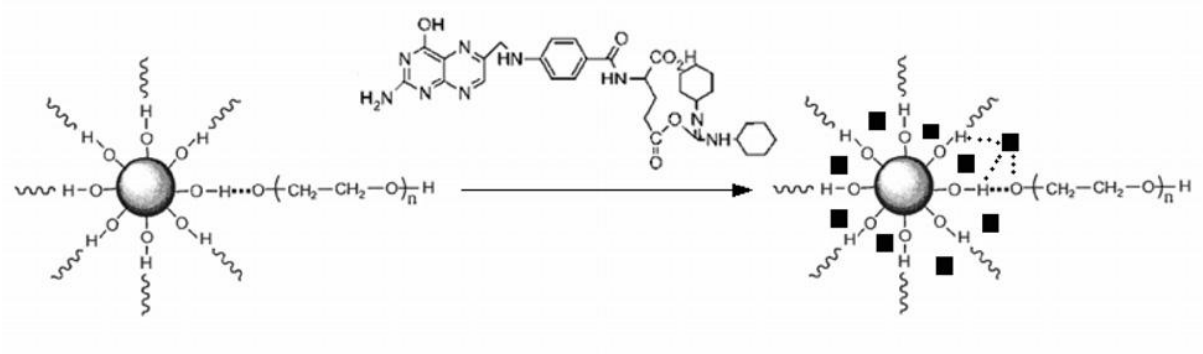

PEG-functionalized Fe_3O_4 Folate modified PEG-functionalized Fe_3O_4

Step 4: Conjugation of drug to functionalize Fe_3O_4

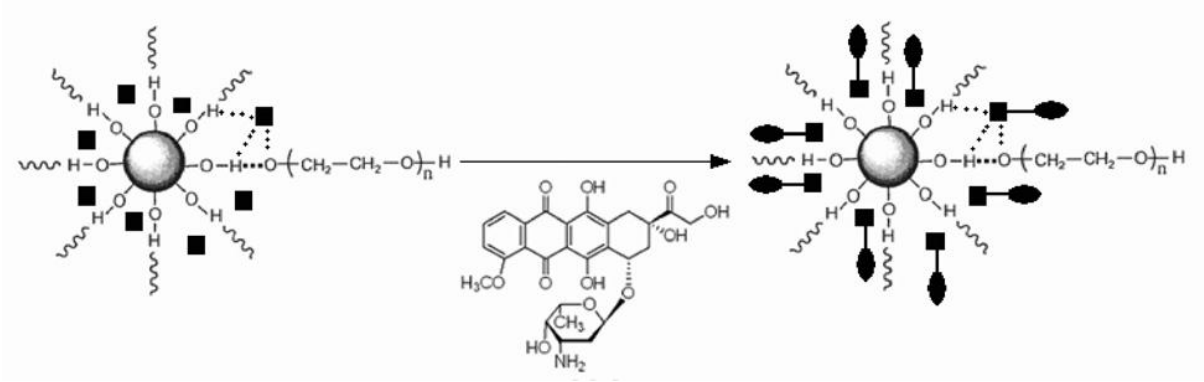

Folate modified PEG-functionalized Fe_3O_4 | Doxorubicin | Drug loaded Folate modified PEG-functionalized Fe_3O_4

3.3 Characterization Techniques

The composition, morphology, magnetic properties, and sizes of the synthesized nanoparticles were analysed by X-ray diffraction, transmission electron microscope, vibrating sample magnetometer, infrared and UV-vis spectroscopy's.

3.3.1 X-ray diffraction (XRD)

X-ray Diffraction (XRD) is a powerful non-destructive technique for characterizing crystalline materials. It provides information on structures, phases, preferred crystal orientations, and other structural parameters, such as average grain size, crystallinity, strain, and crystal defects. X-ray diffraction peaks are produced by constructive interference of monochromatic beam of x-rays scattered at specific angles from each set of lattice planes in a sample. The phenomenon is called X-ray diffraction.

3.3.1.1 Working

X ray diffractometers consist of three basic elements: an X-ray tube, a sample holder, and an X-ray detector. X-rays are generated in a cathode ray tube by heating a filament to produce electrons, accelerating the electrons toward a target by applying a

voltage, and bombarding the target material with electrons. When electrons have sufficient energy to dislodge inner shell electrons of the target material, characteristic X-rays are produced. These spectra consist of several components, the most common being K_α and K_β. K_α consists, in part, of $K_{\alpha1}$ and $K_{\alpha2}$. $K_{\alpha1}$ has a slightly shorter wavelength and twice the intensity as $K_{\alpha2}$. The specific wavelengths are characteristic of the target material (Cu, Fe, Mo, and Cr).

Filtering, by foils or crystal monochrometers, is required to produce monochromatic X-rays needed for diffraction. $K_{\alpha1}$and $K_{\alpha2}$ are sufficiently close in wavelength such that a weighted average of the two is used. Copper is the most common target material for single-crystal diffraction, with Cu K_α radiation, λ = 1.54056 Å. These X-rays are collimated and directed onto the sample. As the sample and detector are rotated, the intensity of the reflected X-rays is recorded.

Figure 3.2 The PANanaltical XRD PROX' pert

When the geometry of the incident X-rays impinging the sample satisfies the Bragg equation, constructive interference occurs and a peak in intensity is observed. A detector records and processes this X-ray signal and converts it to a count rate which is then output to a device such as a printer or computer monitor. The geometry of an X-ray diffractometer is such that the sample rotates in the path of the collimated X-ray

beam at an angle θ while the X-ray detector is mounted on an arm to collect the diffracted X-rays and rotates at an angle of 2θ. The instrument used to maintain the angle and rotate the sample is termed a *goniometer.*

When an X-ray beam hits a sample and is diffracted, we can measure the distances between the planes of the atoms that constitute the sample by applying the Bragg's Law.

$$n\lambda = 2d\sin\theta,$$

Where n is an integer, λ is the wavelength of incident wave, d is the lattice spacing and θ is the angle between the incident ray and the scattering planes. The characteristic set of d-spacings generated in a typical X-ray scan provides a unique "fingerprint" of the compound. When properly interpreted, by comparison with standard reference patterns, this "fingerprint" allows for identification of the material [66].

3.3.1.2 Applications

1) To determine crystal structure
2) To determine lattice parameters, strain, grain size, epitaxy, phase composition, preferred orientation order disorder transformation, thermal expansion etc
3) To identify crystalline phases and orientation
4) To measure thickness of thin films and multi-layers

The crystallite size can be easily calculated by Scherrer equation

$$\mathbf{D = k\lambda/B\cos\theta}$$

Here, the X-ray wavelength of CuK_{α} radiation λ is 1.54056 Å, k is the shape factor which can be assigned a value of 0.9 if the shape is spherical, θ is Bragg angle and β is the full width at half maximum in radians.

3.3.2 Transmission Electron Microscope (TEM)

Transmission electron microscopy (TEM) has become a major support tool in the list of characterization techniques for materials scientists. TEM's has high lateral spatial resolution (better than 0.2 nm "point-to-point'') and it has capability to produce both image and diffraction information from a single sample. In addition, the highly energetic beam of electrons used in TEM interacts with sample matter to produce characteristic radiation. These signals are analyzed to determine materials characterization.

3.3.2.1 Principle of operation

The transmission electron microscope (TEM) forms an image by accelerating a beam of electrons that pass through the specimen. In TEM, electrons are accelerated to 100 KeV or higher (up to 1MeV), projected onto a thin specimen (less than 200 nm) by means of the condenser lens system, and penetrate the sample thickness either undeflected or deflected. The greatest advantages that TEM offers are the high magnification ranging from 50 to 10^6 and its ability to provide both image and diffraction information from a single sample.

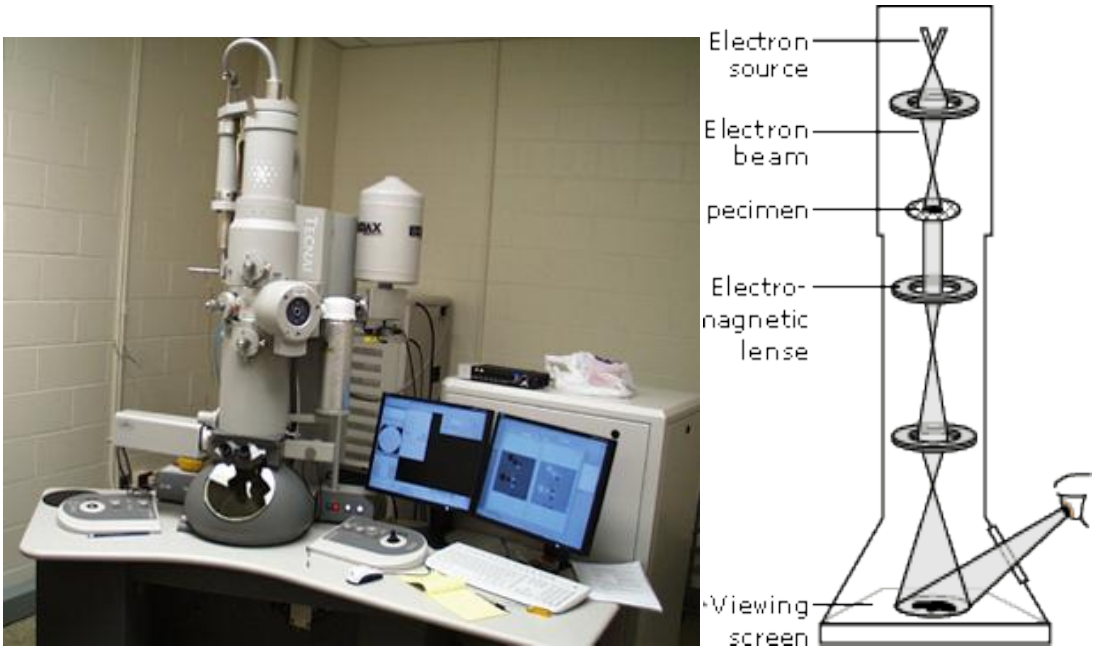

Figure 3.3 (a) FEITecnai T12 S/TEM (b) Schematic ray diagram of TEM

The scattering processes experienced by electrons during their passage through the specimen determine the kind of information obtained. Elastic scattering involves no energy loss and gives rise to diffraction patterns. Inelastic interactions between primary electrons and sample electrons at heterogeneities such as grain boundaries, dislocations, second phase particles, defects, density variations, etc., cause complex absorption and scattering effects, leading to a spatial variation in the intensity of the transmitted electrons. In TEM one can switch between imaging the sample and viewing its diffraction pattern by changing the strength of the intermediate lens.

One short coming of TEM is its limited depth resolution. Electron scattering information in a TEM image originates from a three-dimensional sample, but is projected onto a two dimensional detector. Therefore, structure information along the electron beam direction is superimposed at the image plane. Although the most difficult aspect of the TEM technique is the preparation of samples.

In addition to the capability of structural characterization and chemical analyses, TEM also has been explored for other applications in nanotechnology. Examples include the determination of melting points of nanocrystals, in which, an electron beam is used to heat up the nanocrystals and the melting points are determined by the disappearance of electron diffraction. Another example is the measurement of mechanical and electrical properties of individual nanowires and nanotubes. This technique allows a one-to-one correlation between the structure and properties of the nanowires [67].

3.3.3 Vibrating sample magnetometer (VSM)

The vibrating sample magnetometer has become a widely used instrument for determining magnetic properties of a large variety of materials: diamagnetic, paramagnetic, ferromagnetic and antiferromagnetic. This experimental technique was invented in 1956 by Simon Foner, a scientist of the MIT.

.

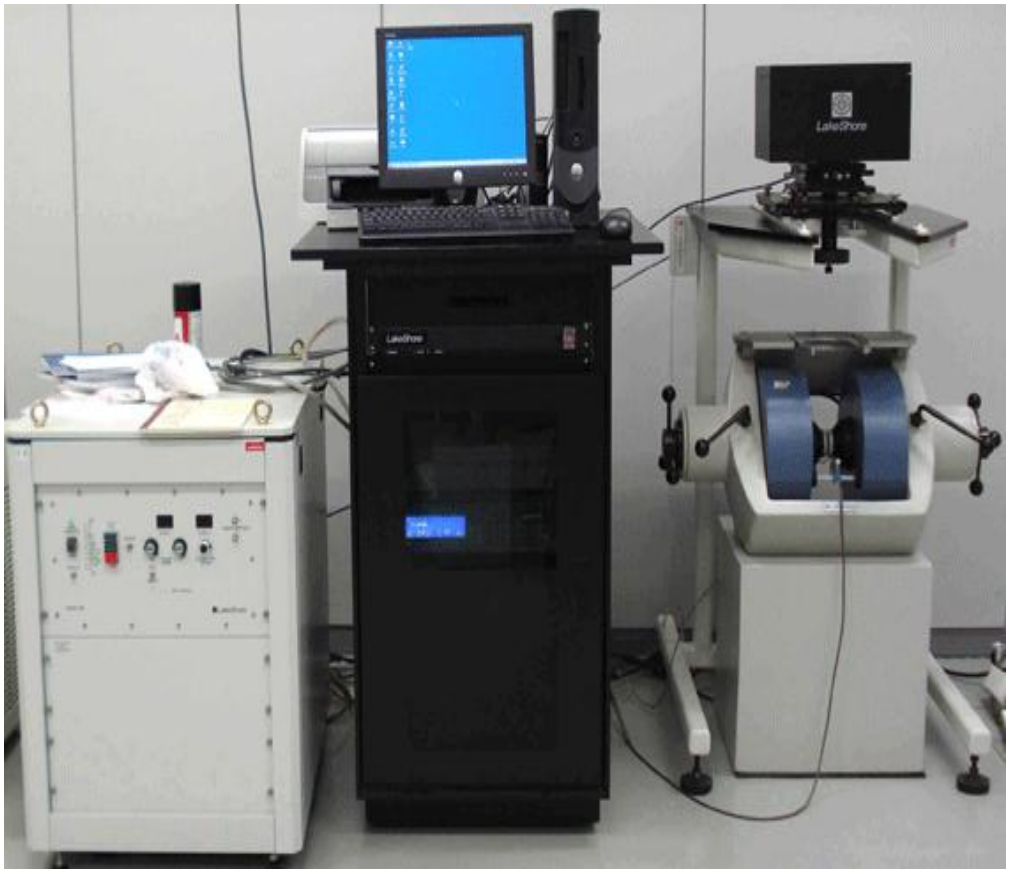

Figure 3.4 VSM Tamakawa model TM-VSM 1230-HHHS

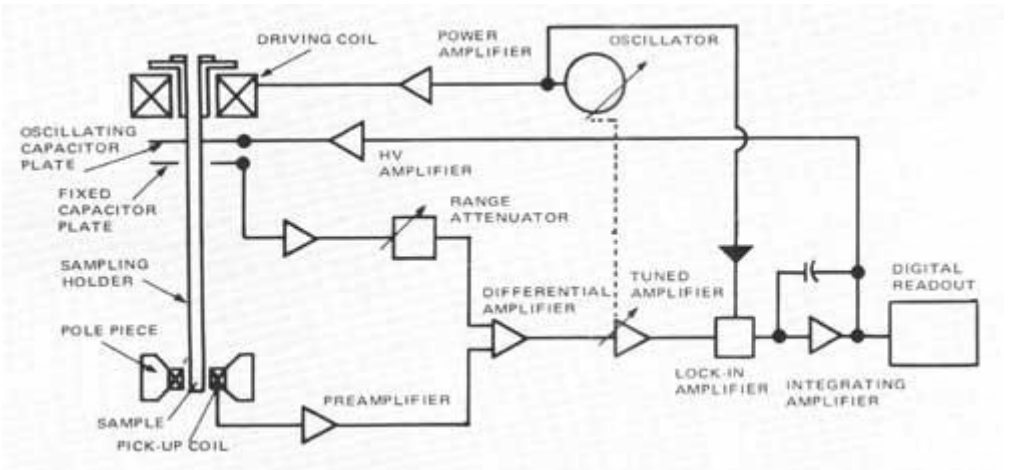

Figure 3.5 Vibrating sample magnetometer block diagram

3.3.3.1 Principle

A vibrating sample magnetometer (VSM) operates on Faraday's Law of Induction, which tells that a changing magnetic field will produce an electric field. This electric field can be measured and can tell us information about the changing magnetic field.

3.3.3.2 Operation

If a sample is placed in a uniform magnetic field, created between the poles of electromagnet, a dipole moment will be induced proportional to the product of the sample susceptibility and the applied field. If the sample vibrates with sinusoidal motion a sinusoidal electrical signal can be induced in pick-up coils. The signal has the same frequency of vibration and its amplitude will be proportional to the magnetic moment.

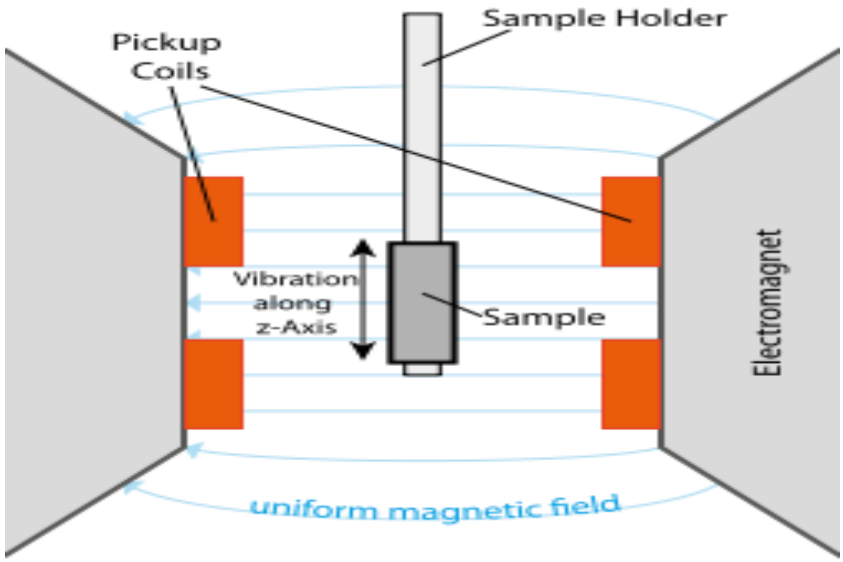

Figure 3.6 Illustration of principle of VSM

The material under study in the VSM is inserted in the sample holder so that it rests centered in a pair of pickup coils between the poles of an electromagnet. The sample holder is mounted using a sample rod in a transducer assembly which passes through

the centre of a driving coil. The transducer is driven by a power amplifier which itself is driven by an oscillator at a frequency of 71 Hertz. The magnetic sample vibrates along the z-axis perpendicular to the magnetizing field. As it does so, it induces a signal in the sample pickup coils as described above. The magnitude of this signal is dependent on the magnetic properties of the sample itself.

Pair of stationary coils picks up the induced ac signal, which is proportional to the amplitude and frequency of the vibration and is used as a control signal for modulation of the transducer. The output of the sample coil is fed to the differential input of a lock-in amplifier. The reference input of the lock-in comes from the sine wave oscillator used to drive the sample holder. The output of the lock-in goes to the data acquisition computer as well as the magnitude of the applied magnetic field coming from a gauss meter. The signal from the lock-in amplifier is directly proportional to the magnetic moment of the sample. The computer is now able to graph the magnetic moment of the sample against the applied magnetic field [68].

3.3.4 Fourier Transform Infrared Spectroscopy (FTIR Spectroscopy)

In infrared spectroscopy, IR radiation is passed through a prepared sample. Some of the infrared radiation isabsorbed by the sample and some of it is passed through (transmitted). The resulting spectrum represents the molecular absorption and transmission, creating a molecular fingerprint of the sample. Like a fingerprint no two unique molecular structures produce the same infrared spectrum. This makes infrared spectroscopy useful for several types of analysis. It can identify their functional groups and their attachment with other groups [69].

3.3.4.1 Instrumentation and Working

The working process is as follows:

1) Source: Infrared energy is emitted from a glowing black-body source. This beam passes through an aperture which controls the amount of energy presented to the sample and ultimately to the detector.

2) Interferometer: The beam enters the interferometer where the "spectral encoding" takes place. The resulting interferogram signal then exits the interferometer.

3) Sample: The beam enters the sample compartment where it is transmitted through or reflected off on the surface of the sample, depending on the type of analysis being accomplished. This is where specific frequencies of energy, which are uniquely characteristic of the sample, are absorbed.

4) Detector: The beam finally passes to the detector for final measurement. The detectors used are specially designed to measure the special interferogram signal.

5) The Computer: The measured signal is digitized and sent to the computer where the Fourier transformation takes place. The final infrared spectrum is then presented to the user for interpretation and any further manipulation.

Because there needs to be a relative scale for the absorption intensity, a background spectrum must also be measured. This is normally a measurement with no sample in the beam. This can be compared to the measurement with the sample in the beam to determine the "percent transmittance."

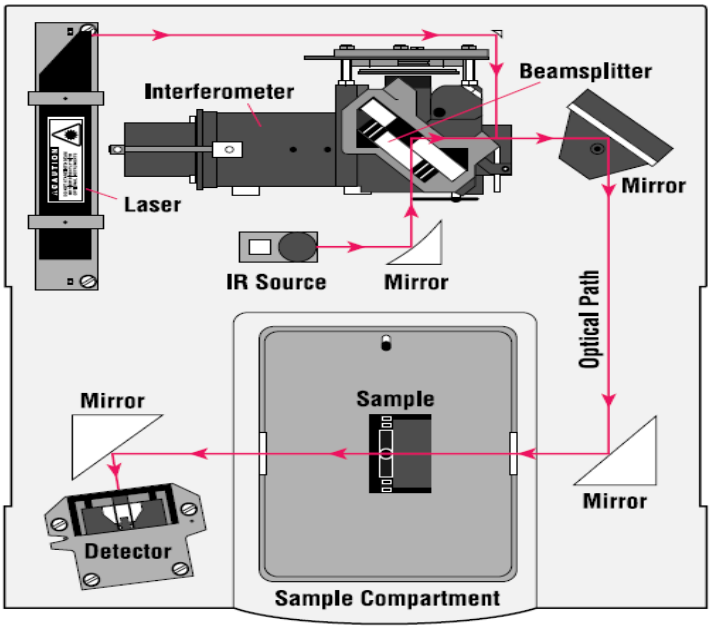

Figure 3.7 FTIR Spectrometer layout

This technique results in a spectrum which has all of the instrumental characteristics removed. Thus, all spectral features which are present are strictly due to the sample. A

single background measurement can be used for many sample measurements because this spectrum is characteristic of the instrument itself.

3.3.4.2 Advantages of FT-IR

Some of the major advantages of FT-IR over the dispersive technique include:

1) Speed: Because all of the frequencies are measured simultaneously, most measurements by FT-IR are made in a matter of seconds rather than several minutes. This is sometimes referred to as the Felgett Advantage.

2) Sensitivity: Sensitivity is dramatically improved with FT-IR for many reasons. The detectors employed are much more sensitive, the optical throughput is much higher (referred to as the Jacquinot Advantage) which results in much lower noise levels, and the fast scans enable the co-addition of several scans in order to reduce the random measurement noise to any desired level (referred to as signal averaging).

3) Mechanical Simplicity: The moving mirror in the interferometer is the only continuously moving part in the instrument. Thus, there is very little possibility of mechanical breakdown.

4) Presence of internally Calibration: These instruments employ a He-Ne laser as an internal wavelength calibration standard (referred to as the Connes Advantage). These instruments are self-calibrating and never need to be calibrated by the user.

These advantages, along with several others, make measurements made by FT-IR extremely accurate and reproducible. Thus, it a very reliable technique for positive identification of virtually any sample. The sensitivity benefits enable identification of even the smallest of contaminants. This makes FT-IR an invaluable tool for quality control quality assurance applications whether it is batch-to-batch comparisons to quality standards or analysis of an unknown contaminant. In addition, the sensitivity and accuracy of FT-IR detectors, along with a wide variety of software algorithms, have dramatically increased the practical use of infrared for quantitative analysis. Quantitative methods can be easily developed and calibrated and can be incorporated into simple procedures for routine analysis.

Thus, the Fourier Transform Infrared (FT-IR) technique has brought significant practical advantages to infrared spectroscopy. It has made possible the development of many new sampling techniques which were designed to tackle challenging problems which were impossible by older technology. It has made the use of infrared analysis virtually limitless.

3.3.5 UV-Visible Spectroscopy

Ultraviolet-visible spectroscopy or ultraviolet-visible spectrophotometry (UV-Vis) refers to absorption spectroscopy in the ultraviolet-visible spectral region. This means it uses light in the visible and adjacent (near-UV and near-infrared (NIR)) ranges. The absorption in the visible range directly affects the perceived colour of the chemicals involved. In this region of the electromagnetic spectrum, molecules undergo electronic transitions. This technique is complementary to fluorescence spectroscopy, in that fluorescence deals with transitions from the excited state to the ground state, while absorption measures transitions from the ground state to the excited state. UV-Vis spectroscopy is routinely used in the quantitative determination of solutions of transition metal ions and highly conjugated organic compounds. Virtually all UV spectra are recorded solution-phase [70].

3.3.5.1 Principle

When a sample of an unknown compound is exposed to light, certain functional groups within the molecule absorb UV light of different wavelengths. In UV-Visible spectroscopy, the term chromophore is used to indicate a functional group that absorbs electromagnetic radiation, usually in the UV or visible region. The type of functional groups that absorb ultraviolet light can be conjugated species, such as alkenes, aromatics, etc., making UV-Visible spectroscopy useful for distinguishing conjugated dienes from conjugated trines, and so forth. Also many metal-ligand complexes also absorb UV-visible light. It’s important to remember that UV-visible EM radiation causes electronic transitions within a molecule, promoting bonding and non-bonding electrons to higher, less stable anti bonding orbitals. The molecule then

loses this excess energy by rotation and vibrational relaxation, but some compounds can lose their energy by emission processes such as fluorescence.

Figure 3.8 UV-Visible Spectrometer

3.3.5.2 Practical Applications of UV-Vis spectroscopy

1) UV was the first organic spectral method; however, it is rarely used as a primary method for structure determination.

2) It is most useful in combination with NMR and IR data to elucidate unique electronic features that may be ambiguous in those methods.

3) It can be used to assay (via l_{max} and molar absorptivity) the proper irradiation wavelengths for photochemical experiments, or the design of UV resistant paints and coatings.

4) The most ubiquitous use of UV is as a detection device for HPLC; since UV is utilized for solution phase samples vs. a reference solvent this is easily incorporated into LC design.

4.1 XRD Analysis

The X-ray diffraction patterns of the magnetite nanoparticles prepared by thermal decomposition and co-precipitation methods and coated with different concentrations of PEG are shown in figure 4.1.

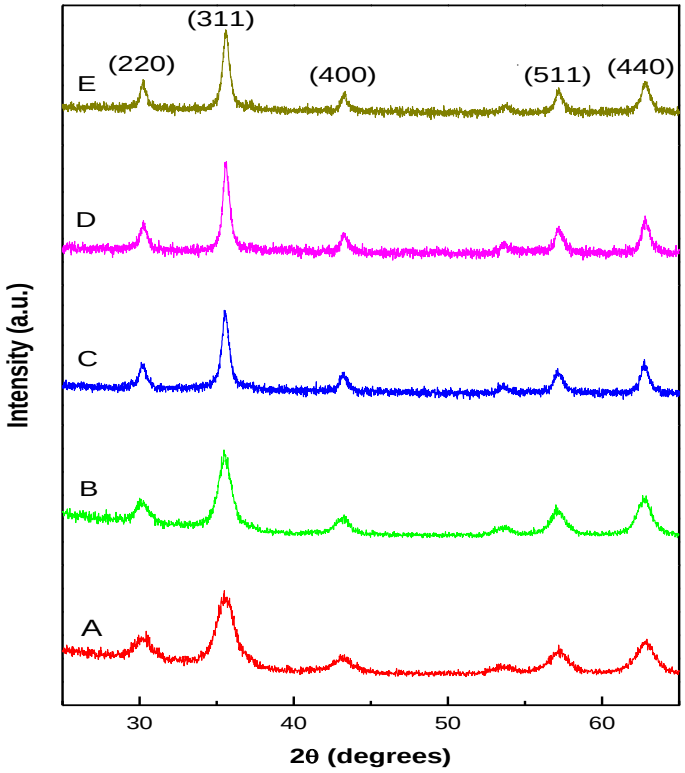

Figure 4.1 XRD spectra of (A) magnetite nanoparticles prepared by thermal decomposition method, (B) magnetite nanoparticles prepared by chemical co-precipitation route, (C) PEG coated magnetite nanoparticles; PEG:Fe_3O_4 (w/w) = 1:2, (D) PEG coated magnetite nanoparticles; PEG:Fe_3O_4 (w/w) = 1:1, (E) PEG coated magnetite nanoparticles; PEG:Fe_3O_4 (w/w) = 1:4

The peaks at 30.4°, 35.5°, 43°, 57.1° and 62.9° correspond to diffraction from the (220), (311), (400), (511) and (440) crystalline planes, respectively. The coincidence

of the diffraction pattern of these nanoparticles with the standard pattern of magnetite indicates that these samples have single phase cubic spinel structure [71] and no other phase is present in these samples. The average crystallite size of magnetite nanoparticles was determined by using classical Scherrer's equation [72]:

$$\mathbf{D = k\lambda / \beta cos\theta}$$

The highest intense reflecting peak corresponding to (311) crystalline plane is used to calculate the average crystallite size. The estimated size of the different samples is listed below in table 4.1 for each sample.

Table 4.1 Crystallite size of as-synthesized and PEG functionalized magnetite nanoparticles

Sample	Crystallite size (nm)
A	7.0
B	9.0
C	17.0
D	18.2
E	18.0

4.2 TEM Analysis

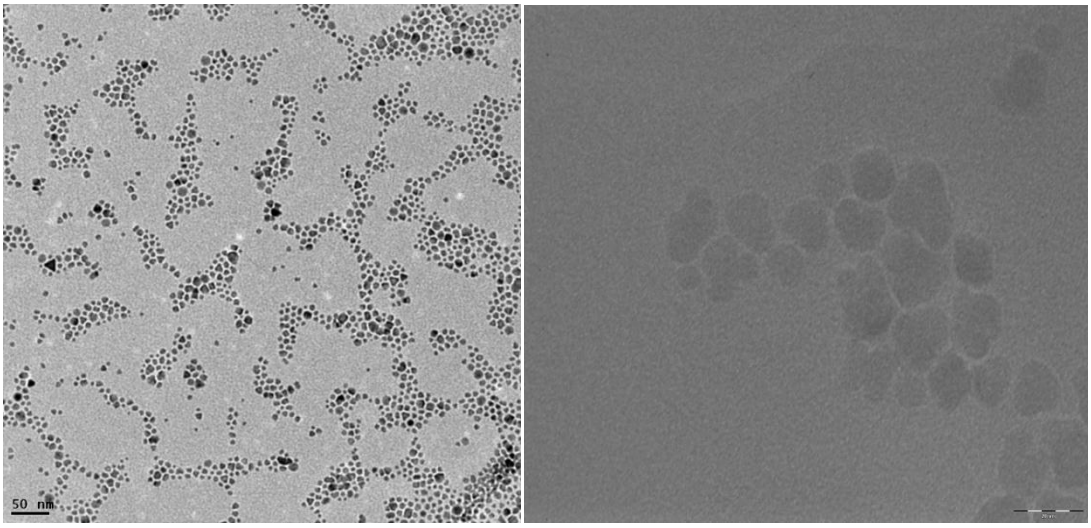

Figure 4.2 TEM images of magnetite nanoparticles prepared by (A) thermal decomposition and (B) co-precipitation method

The particle size and particle morphology of magnetite nanoparticles were studied by transmission electron microscopy. A representative TEM image of magnetite nanoparticles prepared by thermal decomposition and co-precipitation routes are shown in figure 4.2.

Figure 4.2 show that magnetite nanoparticles prepared by thermal decomposition are monodisperse while that prepared from co-precipitation are polydisperse in nature with near spherical morphology. The average particle size obtained from TEM is in good agreement with that calculated by Scherrer's formula according to the XRD pattern of magnetite nanoparticles prepared by thermal decomposition.

4.3 Fourier transform infrared spectroscopy (FTIR)

To characterize the surface chemical functionality of nanostructures, infrared spectra of magnetite nanoparticles, PEG coated magnetite nanoparticles and Folic acid modified, PEG coated magnetite nanoparticles were obtained by the KBr pellet method. In this method, the solid sample is finely pulverized with pure, dry KBr, the mixture is pressed in a hydraulic press to form a transparent pellet, and the spectrum of the pellet is measured. Background measurements were performed with KBr powder before the analysis of the samples. Spectra were collected between 4000 to 400 cm^{-1} at a resolution of 4 cm^{-1}.

4.3.1 FTIR analysis of monodisperse magnetite nanoparticles

Infrared spectra of magnetite nanoparticles, PEG coated magnetite nanoparticles and folic acid modified, PEG coated magnetite nanoparticles are shown in figure 4.3. The FTIR spectra of folic acid and PEG 600 are also shown as reference in figure 4.3. The interpretation of each FTIR spectrum is given in table 4.2. Based on the assignment of the FTIR spectra of magnetite reported in the literature [73, 74], the characteristic absorption bands at 630 and 587cm^{-1} of curve C are attributed to Fe-O bonds. The two bands at 630 and 587 cm^{-1} are a consequence of the splitting of the absorption band of the Fe-O bond of bulk magnetite at 570 cm^{-1} that shifts to a higher wavenumber. This confirms the presence of magnetite nanoparticles in the sample.

The absorption bands at 1115 and 1384 cm^{-1} corresponds to C-O-C ether symmetric and asymmetric stretching vibrations, respectively. The absorption bands at 2923 and 2853 cm^{-1} correspond to –CH symmetric and asymmetric stretching vibrations, respectively. The absorption band at 3425 cm^{-1} is attributed to hydroxyl (OH) stretching vibration. This confirms that PEG was coated on the surface of magnetite nanoparticles [65].

The characteristic FTIR absorption band of folic acid was observed at 1631 cm^{-1} which was attributed to -C=N stretching vibration. This confirms that folic acid is chemically conjugated with PEG coated magnetite nanoparticles. The absorption band at 1047 cm^{-1} is due to C-N stretching vibration originated from oleylamine [69]. The absorption band at 2360 cm^{-1} is attributed to the presence of CO_2 in the measuring chamber of the device in which the specimen was placed, and is part of the equipment's background noise.

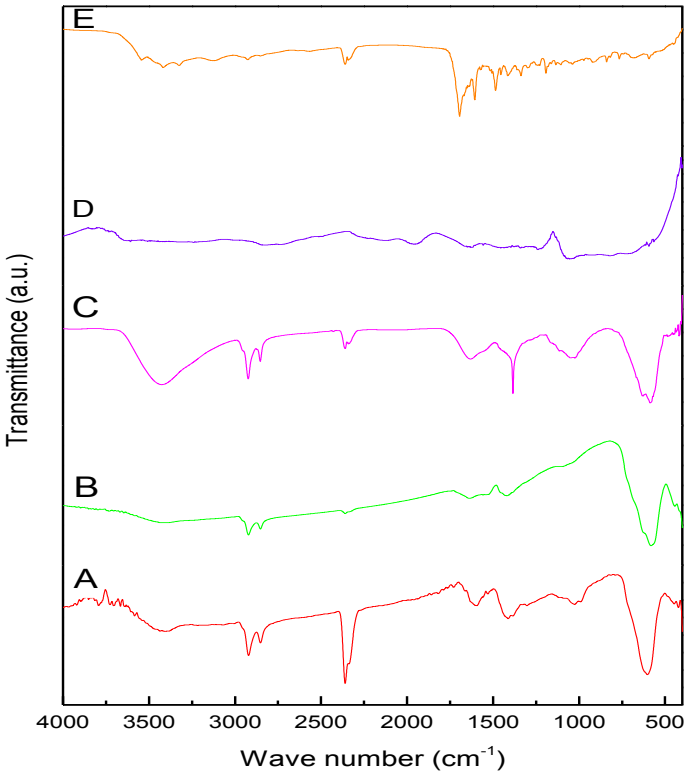

Figure 4.3 FTIR spectra of (A) magnetite nanoparticles, (B) PEG coated magnetite nanoparticles, (C) FA modified, PEG coated magnetite nanoparticles, (D) pure PEG 600, (E) pure Folic acid

Table 4.2 Interpretation of the FTIR spectra of different samples

Sample	Peak position (cm^{-1})	Interpretation
(A)	3409	-NH_2stretching
	2922	C-H asymmetric stretching
	2851	C-H symmetric stretching
	2360	Molecular vibration of CO_2
	603	Fe-O stretching
(B)	2922	C-H asymmetric stretching
	2852	C-H symmetric stretching
	2359	Molecular CO_2
	1098	C-O-C stretching
	582	Fe-O stretching
(C)	3425	O-H stretching
	2923	C-H asymmetric stretching
	2853	C-H symmetric stretching
	2360	Molecular CO_2vibration
	1631	C=N stretching
	1384	C-O-C asymmetric stretching
	1115	C-O-C symmetric stretching
	1047	C-N stretching
	630 and 587	Fe-O stretching
(D)	2845	C-H symmetric stretching
	1050	C-O-C symmetric stretching
(E)	3551	N-H stretching
	2360	Molecular CO_2
	1680	C=O stretching (carboxyl group)
	1606	NH- bending mode
	1486	Phenyl ring

4.3.2 FTIR analysis of PEG coated polydisperse magnetite nanoparticles

The FTIR spectra of the magnetite nanoparticles coated with different concentrations of PEG are shown in figure 4.4. The absorption bands observed due to PEG are already explained in section 4.3.1. The absorption bands observed at 1628 and 1625

cm^{-1} in the samples can be attributed to molecular H_2O bending mode. The absorption bands observed at 1417 and 1412 cm^{-1} in the samples can be attributed to $–NH_3^+$ asymmetric stretching vibration, respectively [69].

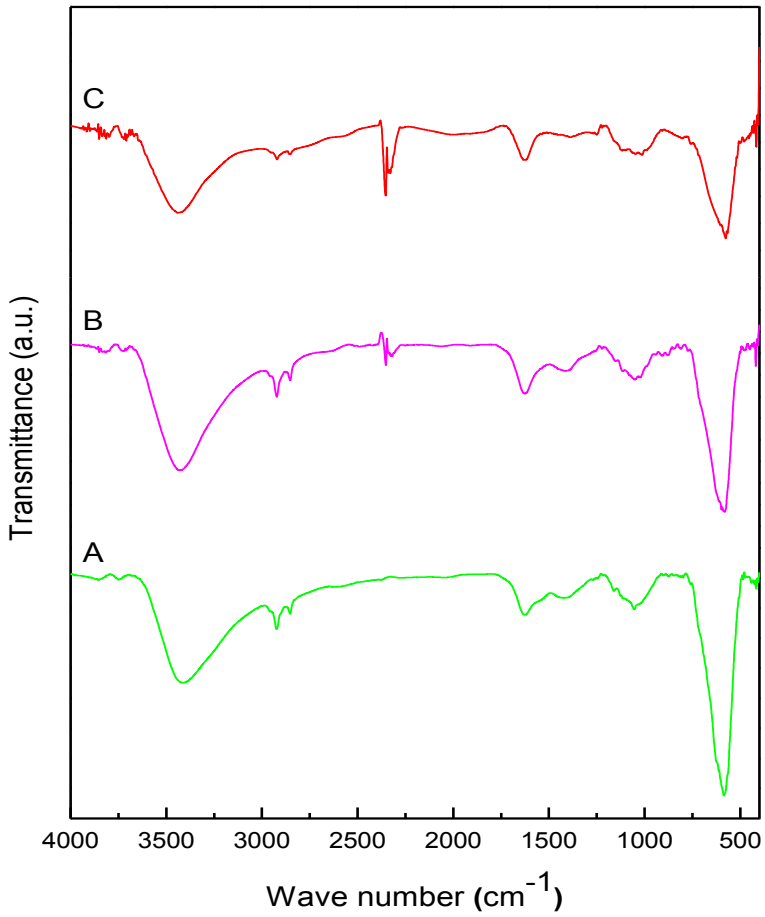

Figure 4.4 FTIR spectra of (A) PEG coated magnetite nanoparticles; PEG:Fe_3O_4 (w/w) = 1:2, (B) PEG coated magnetite nanoparticles; PEG:Fe_3O_4 (w/w) = 1:1, (C) PEG coated magnetite nanoparticles; PEG:Fe_3O_4 (w/w) = 1:4

The FTIR spectra of magnetite nanoparticles coated with different concentrations of PEG 600 are interpreted in table 4.3.

Table 4.3 Interpretation of the FTIR spectra of PEG coated magnetite nanoparticles

Sample (A) Peak position (cm^{-1})	Sample (B) Peak position (cm^{-1})	Sample (C) Peak position (cm^{-1})	Interpretation
3414	3428	3440	O-H stretching
2923	2922	2921	C-H symmetric stretching
2852	2853	2853	C-H symmetric stretching
2352	2352	2353	Molecular CO_2
1625	1625	1628	Molecular H_2O vibration
1412	1417	1412	$–NH_3^+$asymmetric stretching
1114	1116	1114	C-O-C symmetric stretching
630 and 586	630 and 581	628 and 576	Fe-O stretching

4.4 UV-Vis Spectrum Analysis

The UV spectrum of doxorubicin loaded FA modified, PEG coated magnetite nanoparticles and pure doxorubicin is shown below in figure 4.5.

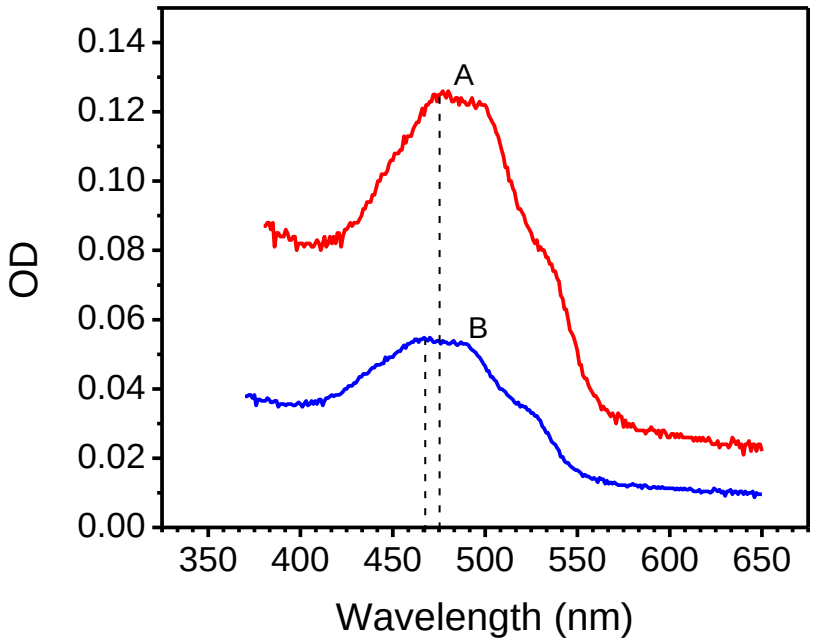

Figure 4.5 UV spectrum of (A) pure doxorubicin and (B) doxorubicin loaded FA modified, PEG coated magnetite nanoparticles

The curve A represents the UV spectra of pure doxorubicin and curve B represents the UV spectra of doxorubicin loaded FA modified, PEG coated magnetite nanoparticles. Pure doxorubicin peak occurs at 477 nm and in FA modified, PEG coated magnetite nanoparticles the doxorubicin peak shifts to 470 nm with a fall in intensity. Thus, from the UV spectra we can say that drug (doxorubicin) is loaded in the sample with a little shift in the peak position.

4.5 VSM Measurements

The VSM measurements of magnetite nanoparticles prepared by thermal decomposition method (A), PEG coated magnetite nanoparticles (B) and FA modified, PEG coated magnetite nanoparticles (C) are shown in figure 4.6.

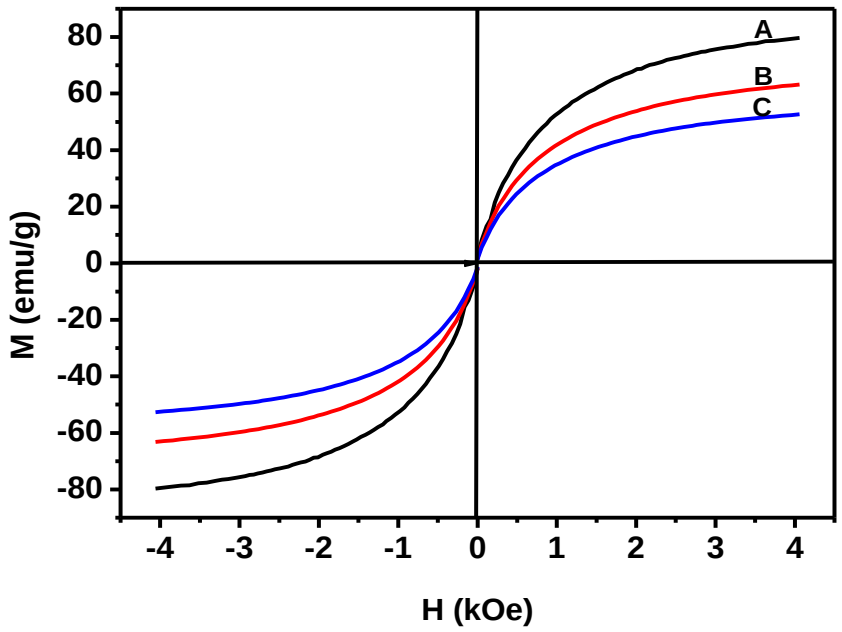

Figure 4.6 Magnetization curves of (A) Fe_3O_4, (B) Fe_3O_4-PEG, (C) Fe_3O_4-PEG-FA

From figure 4.6, it is clear that as the magnetic field increases, the magnetization of all samples increases and saturates at higher field, which is a typical characteristic of superparamagnetic particles. The saturation magnetizations of different samples are listed in table 4.4.

Table 4.4 Saturation magnetizations of Fe_3O_4, Fe_3O_4-PEG and Fe_3O_4-PEG-FA

Sample	Saturation magnetization (in emu/g)
Fe_3O_4	79.7
Fe_3O_4-PEG	63.2
Fe_3O_4-PEG-FA	52.7

It can be observed from table 4.4 that the saturation magnetization of the nanoparticles decreases upon coating. This can be due to the fact that polymer coating will provide greater diamagnetic contribution to the sample.

4.6 Conclusions

- Magnetite nanoparticles were synthesized by chemical co-precipitation and thermal decomposition routes.
- Magnetite nanoparticles have a large surface/volume ratio and tend to agglomerate to reduce their surface energy. To prevent the particle agglomeration and to provide biocompatibility to drug delivery system, magnetite nanoparticles were coated with hydrophilic polymer PEG.
- To achieve specific targeting, nanoparticles were coated with folic Acid (FA). It will increase the cancer cell recognition and intracellular uptake of drug delivery systems in tumor environment.
- The anticancer drug doxorubicin was loaded in FA functionalized, PEG coated magnetite nanostructures.
- X-ray diffraction studies indicate that magnetite nanoparticles have single phase cubic inverse spinel structure and no other phases were detected, which confirms the structural purity of the magnetic nanoparticles.
- TEM analysis indicates that magnetite nanoparticles synthesized by thermal decomposition were monodisperse in nature with nearly spherical

morphology, having average size of 6.6 nm, while the co-precipitation method yields polydispersed nanoparticles.

- FTIR analysis indicates that PEG and FA were functionalized on the surface of magnetite nanoparticles.
- UV analysis confirms that anticancer drug (doxorubicin) was loaded in FA modified, PEG coated magnetite nanostructures.
- VSM analysis reveals that saturation magnetization of magnetite nanoparticles is quite high (80 emu/g). This is significantly higher than reported for magnetite nanoparticles prepared by co-precipitation route (60 emu/g). The magnetization of composite system decreases upon functionalization. This is because of the diamagnetic contribution of polymers. However, FA functionalized, PEG coated magnetite nanostructures have saturation magnetization 53 emu/g, which is sufficient for all practical application in magnetic drug targeting.

REFERENCES

1) Beardsley T., A War not Won, *Sci Am 270*, 130-138 (1994).
2) Jain R. K., Delivery of Molecular and Cellular Medicine to Solid Tumors, *Adv Drug Deliv Rev 46*, 149-168 (2001).
3) Jang S. H., Wientjes M. G., Lu D., Au J. L., Drug Delivery and Transport to Solid Tumors, *Pharm Res 20*, 1337-1350 (2003).
4) Hanahan D., Weinberg R.A., The hallmarks of cancer, Cell 100: 57–70 (2000).
5) T Lammers, WE Hennink, G Storm, Tumour-targeted nanomedicines: principles and practice, British Journal of Cancer (2008) 99, 392 – 397.
6) Fabrizio Marcucci and François Lefoulon, Active targeting with particulate drug carriers in tumor therapy: fundamentals and recent progress, DDT Vol. 9, No. 5, March 2004.
7) Jaspreet K. Vasir, Vinod Labhasetwar, Targeted Drug Delivery in Cancer Therapy, *Technology in Cancer Research & Treatment, ISSN 1533-0346, Volume 4, Number 4, August (2005).*
8) Au J. L., Jang S. H., Zheng J., Chen C. T., Song S., Hu L., Wientjes M. G., Determinants of Drug Delivery and Transport to Solid Tumors, *J Control Release 74*, 31-46 (2001).
9) Ehrlich P., The collected papers of Paul Ehrlich, Pergamon, London, (1960).
10) Moghimi S. M. et al., Pharmacol. Rev. (2001) 53 (2), 283.
11) Maeda H, Wu J, Sawa T, Matsumura Y, Hori K (2000), Tumour vascular permeability and the EPR effect in macromolecular therapeutics: a review, J Control Release 65 (2000) : 271–284.
12) Au J. L., Jang S. H., Wientjes M. G., Clinical Aspects of Drug Delivery to Tumors, *J Control Release 78*, 81-95 (2002).
13) Sledge Jr. G. W. and Miller K. D., Eur. J. Cancer (2003) 39 (12), 1668.
14) Teicher B. A., Drug. Resist. Updat. (2000) 3 (2), 67.
15) Rubin P., Casarett G., Microcirculation of Tumors, *Clin Radiol 17*, 220-229 (1966).
16) Shubik P., Vascularization of Tumors: A Review, *J Cancer Res Clin Oncol 103*, 211-226 (1982).

17) Hobbs S. K., Monsky W. L., Yuan F., Roberts W. G., Griffith L., Torchilin V. P., Jain R. K., Regulation of Transport Pathways in Tumor Vessels: Role of Tumor Type and Microenvironment, *Proc Natl Acad Sci USA 95*, 4607-4612 (1998).
18) Yuan F., Salehi H. A., Boucher Y., Vasthare U. S., Tuma R. F., Jain R. K., Vascular Permeability and Microcirculation of Gliomas and Mammary Carcinomas Transplanted in Rat and Mouse Cranial Windows, *Cancer Res 54*, 4564-4568 (1994).
19) Dellian M., Witwer B. P., Salehi H. A., Yuan F., Jain R. K., Quantitation and Physiological Characterization of Angiogenic Vessels in Mice: Effect of Basic Fibroblast Growth Factor, Vascular Endothelial Growth Factor/Vascular Permeability Factor, and Host Microenvironment, *Am J Pathol 149*, 59-71 (1996).
20) Maeda H., Wu J., Sawa T., Matsumura Y., Hori K., Tumor Vascular Permeability and the EPR Effect in Macromolecular Therapeutics: A Review, *J Control Release 65*, 271-284 (2000).
21) Matsumura Y., Maeda H., A New Concept for Macromolecular Therapeutics in Cancer Chemotherapy: Mechanism of Tumoritropic Accumulation of Proteins and the Antitumor Agent Smancs, *Cancer Res 46*, 6387-6392 (1986).
22) Duncan R., Sat Y. N, Tumor Targeting by Enhanced Permeability and Retention (EPR) Effect, *Ann. Oncol. 9*, 39 (1998).
23) Gregoriadis G., Engineering Liposomes for Drug Delivery: Progress and Problems, *Trends Biotechnol 13*, 527-537 (1995).
24) Zlotecki R. A., Boucher Y., Lee I., Baxter L. T., Jain R. K., Effect of Angiotensin II Induced Hypertension on Tumor Blood Flow and Interstitial Fluid Pressure, *Cancer Res 53*, 2466-2468 (1993).
25) Allen TM, Ligand-targeted therapeutics in anticancer therapy, Nat Rev Cancer 2: 750–763 (2000).
26) Park JW, Benz CC, Martin FJ, Future directions of liposome and immune liposome-based cancer therapeutics, Semin Oncol 31-S13: 96–205 (2004).
27) Rajgopal A. et al., Biochim. Biophys, Acta (2001) 1537 (3), 175.
28) Sudimack J. and Lee R. J., Adv. Drug Deliv. Rev., (2000) 41 (2), 147.
29) Lu YJ, Low PS, Adv Drug Del Rev, 2002; 54:675–93.

30) Toffoli G, Cernigoi C, Russo A, Gallo A, Bagnoli M, Boiocchi M, Int J Cancer, (1997) ;74:193–8.
31) Lee RJ, Low PS, Biochim Biophys Acta 1233:134–44 (1995).
32) Saul JM, Annapragada A, Natarajan JV, Bellamkonda RV, J Control Release, 92:49–67 (2003).
33) Leamon CP, Cooper SR, Hardee GE, Bio conj Chem, 14:738–47 (2003).
34) Pan XQ, Zheng X, Shi GF, Wang HQ, Ratnam M, Lee RJ, Blood, 100:594–602 (2002).
35) Pan XQ, Wang HQ, Lee RJ, Pharm Res; 20:417–22 (2003).
36) Goren D, Horowitz AT, Tzemach D, Tarshish M, Zalipsky S, Gabizon A, Clin Cancer Res; 6:1949–57 (2000).
37) U.O. Häfeli, Magnetically modulated therapeutic systems, International Journal of Pharmaceutics, 277 (2004) 19–24.
38) LübbeA.S., Bergemann C., Riess H., Clinical experiences with magnetic drug targeting: A phase I study with 4-epidoxorubicin in 14 patients with advanced solid tumors, Cancer Res. 56, 4686–4693 (1996).
39) Goodwin S., Magnetic targeted carriers offer site-specific drug delivery, Oncol. News Int. 9, 22 (2000).
40) Johnson J., Kent T., Koda J., Peterson C., Rudge S., Tapolsky G., The MTC technology: a platform technology for the site-specific delivery of pharmaceutical agents, Eur. Cells Mater, 3 (2002), 12–15.
41) Babincova M, Leszczynska D, Sourivong P and Babinec P, Selective treatment of neoplastic cells using ferritin-mediated electromagnetic hyperthermia, *Med. Hypoth.* , 54,177–9 (2000).
42) Jordan A., Wust P., Fahling H., John W., Hinz A., Felix R., Inductive heating of ferrimagnetic particles and magnetic fluids: physical evaluation of their potential for hyperthermia, Int. J. Hyperthermia 9, 51–68 (1993).
43) Chan D.C.F., Kirpotin D.B., Bunn P.A., Synthesis and evaluation of colloidal magnetic iron oxides for the site-specific radio frequency-induced hyperthermia of cancer, J. Magn. Mater, 122, 374–378 (1993).
44) Jordan A., Scholz R., Maier-Hauff K., Presentation of a new magnetic field therapy system for the treatment of human solid tumors with magnetic fluid hyperthermia, J. Magn. Mater, 225, 118–126 (2001).

45) Moroz P., Jones S.K., Gray B.N., Tumor response to arterial embolization hyperthermia and direct injection hyperthermia in a rabbit liver tumor model, J. Surg. Oncol. 80, 149–156 (2002).
46) Kuznetsov A.A., Shlyakhtin O.A., Brusentsov N.A., Kuznetsov O.A., "Smart" mediators for self-controlled inductive heating, Eur. Cells Mater. 3, 75–77 (2002).
47) Edelman E.R., Langer R., Optimization of release from magnetically controlled polymeric drug release devices, Biomaterials 14, 621–626 (1993).
48) Kost J., Wolfrum J., Langer R., Magnetically enhancedinsulin release in diabetic rats, J. Biomed. Mater.Res. 21, 1367–1373 (1987).
49) Chen H., Langer R., Magnetically-responsive polymerized liposomes as potential oral delivery vehicles, Pharm. Res. 14, 537–540 (1997).
50) Häfeli U.O., Radioactive magnetic microspheres In:Arshady, R. (Ed.), Microspheres, Microcapsules & Liposomes: Magneto and Radio Pharmaceuticals, vol. 3, Citus Books,London, Chapter 18, pp. 559–584 (2001).
51) Scherer F., Anton M., Schillinger U., Magnetofection: enhancing and targeting gene delivery by magnetic force in vitro and in vivo, Gene Therapy 9, 102–109 (2002).
52) Flores G.A., Liu J., In vitro blockage of a simulated vascular system using magneto rheological fluids as a cancer therapy, Eur. Cells Mater. 3, 9–11 (2002).
53) Dailey J.P., Phillips J.P., Li C., Riffle J.S., Synthesis of silicone magnetic fluid for use in eye surgery, J. Magn. Mater.194, 140–148 (1999).
54) Hyuk Sang Yoo, Eun Ah Lee, Tae Gwan Park, Doxorubicin-conjugated biodegradable polymeric micelleshaving acid-cleavable linkages, Journal of Controlled Release 82 (2002).
55) Ka Eul Lee, Byoung Ki Kim, and Soon Hong Yuk, Biodegradable Polymeric Nanospheres Formed by Temperature-Induced Phase Transition in a Mixture of Poly(lactide-co-glycolide) and Poly(ethylene oxide)-Poly(propylene oxide)-Poly(ethylene oxide) Triblock Copolymer, Biomacromolecules 3, 2002.
56) Mohammed Shameem, Heeyong Lee, and Patrick P. DeLuca., A Short-term (Accelerated Release) Approach to Evaluate Peptide Release from PLGA Depot Formulations, *AAPS Pharmsci* (1999); 1 (3) article 7.

57) Khaled Greisha, Tomohiro Sawab, Jun Fangc, Takaaki Akaikea, Hiroshi Maeda, SMA–doxorubicin, a new polymeric micellar drug for effective targeting to solid tumours, Journal of Controlled Release 97 (2004).

58) D. Klose, F. Siepmann, K. Elkharraz, S. Krenzlin, J. Siepmann, How porosity and size affect the drug release mechanisms from PLGA-based microparticles, International Journal of Pharmaceutics 314 (2006).

59) S Purushotham, PEJ Chang, H Rumpel, IHC Kee, R THNg, PKH Chow, C K Tan and R V Ramanujan, Thermo responsive core–shell magnetic nanoparticles for combined modalities of cancer therapy, Nanotechnology 20 (2009).

60) Banu S. Zolnik, Pauline E. Leary, Diane J. Burgess, Elevated temperature accelerated release testing of PLGA microspheres, Journal of Controlled Release 112 (2006).

61) Yong-kyu Lee, Preparation and Characterization of Folic Acid Linked Poly(L-glutamate) nanoparticles for Cancer Targeting, Macromolecular Research, Vol. 14.

62) F H Chen and Q Gao, The grafting and release behaviour of doxorubicin from Fe_3O_4@SiO_2 core–shell structure nanoparticles via an acid cleaving amide bond: the potential for magnetic targeting drug delivery, IOP PUBLISHING, Nanotechnology 19(2008).

63) Torchilin V P, Drug Targeting, *Eur. J. Pharm. Sci.* **11** S81–91 (2000).

64) Yong Zhang, Conroy Sun, Nathan Kohlar and Miqin Zhang, Self-assembled coatings on individual monodispersed magnetite nanoparticles for efficient intracellular uptake, Biomedical microdevices 6:1, 33-40 (2004).

65) J. Zhang, S. Rana, R.S. Srivastava, R.D.K. Misra, On the chemical synthesis and drug delivery response of folate receptor-activated, polyethylene glycol-functionalized magnetite nanoparticles, Acta Biomaterialia 4 (2008) 40–48.

66) B Cullity Elements of X-ray diffraction, 2nd Ed Addison - Wesley publication company, USA (1978).

67) D Williams, C Carter, Transmission Electron Microscopy: A text book for Materials Science, Springer, USA (2009).

68) B D Cullity, Introduction to magnetic materials, Addison-Wesley Publication Company, UK (1972).

69) FTIR Spectroscopy from Wikipedia, the free encyclopaedia.

70) UV-Visible Spectroscopy from Wikipedia, the free encyclopaedia.
71) Cheng F Y, Su C H, Yang Y S, Yeh C S, Tsai C Y, Wu C L, Wu M T and Shieh D B, *Biomaterials* **26 (**2005),729.
72) Hammond C, *The Basics of Crystallography and Diffraction*, (Oxford: Oxford University Press), (1997).
73) Yamaura M, Camilo RL, Sampaio LC, Macedo MA, Nakamura M, Toma HE, Preparation and characterization of (3-aminopropyl) triethoxysilane-coated magnetic nanoparticles, J Mag Magn Mater (2004);279:210.
74) Ma M, Zhang Y, Yu W, Shen HY, Zhang HQ, Gu N, Colloids and Surfaces, Physico chem. Eng Aspects (2003); 212:219.